

Identifying Energy-Dependent Flavor Transitions in High-Energy Astrophysical Neutrino Measurements

Qinrui Liu,^{1,2,3,*} Damiano F. G. Fiorillo,^{4,†} Carlos A. Argüelles,^{5,‡}
Mauricio Bustamante,^{4,§} Ningqiang Song,^{6,7,¶} and Aaron C. Vincent^{1,2,3,**}

¹*Department of Physics, Engineering Physics and Astronomy,
Queen's University, Kingston ON K7L 3N6, Canada*

²*Arthur B. McDonald Canadian Astroparticle Physics Research Institute, Kingston ON K7L 3N6, Canada*

³*Perimeter Institute for Theoretical Physics, Waterloo ON N2L 2Y5, Canada*

⁴*Niels Bohr International Academy, Niels Bohr Institute,
University of Copenhagen, 2100 Copenhagen, Denmark*

⁵*Department of Physics & Laboratory for Particle Physics and Cosmology,
Harvard University, Cambridge, MA 02138, USA*

⁶*Institute of Theoretical Physics, Chinese Academy of Sciences, Beijing, 100190, China*

⁷*Department of Mathematical Sciences, University of Liverpool, Liverpool, L69 7ZL, United Kingdom*
(Dated: December 14, 2023)

The flavor composition of TeV–PeV astrophysical neutrinos, *i.e.*, the proportion of neutrinos of different flavors in their flux, is a versatile probe of high-energy astrophysics and fundamental physics. Because flavor identification is challenging and the number of detected high-energy astrophysical neutrinos is limited, so far measurements of the flavor composition have represented an average over the range of observed neutrino energies. Yet, this washes out the potential existence of changes in the flavor composition with energy and weakens our sensitivity to the many models that posit them. For the first time, we measure the energy dependence of the flavor composition, looking for a transition from low to high energies. Our present-day measurements, based on the 7.5-year public sample of IceCube High-Energy Starting Events (HESE), find no evidence of a flavor transition. The observation of HESE and through-going muons jointly by next-generation neutrino telescopes Baikal-GVD, IceCube-Gen2, KM3NeT, P-ONE, TAMBO, and TRIDENT may identify a flavor transition around 200 TeV by 2030. By 2040, we could infer the flavor composition with which neutrinos are produced with enough precision to establish the transition from neutrino production via the full pion decay chain at low energies to muon-damped pion decay at high energies.

I. INTRODUCTION

In astrophysics, neutrinos hold an esteemed position as compelling messengers from the cosmos. Their minute interaction cross sections [1] make these elusive particles nearly impossible to stop or deflect en route to Earth, allowing them to convey astrophysical information directly from their sources, even if these are embedded in dense environments or produced cosmological distances away. As a consequence, the study of neutrinos provides an invaluable and unique perspective on the most energetic phenomena in the Universe [2–10] and a handle on new physics beyond the reach of terrestrial experiments [8, 9, 11–15].

Over the past decade, IceCube [22] and other neutrino observatories [23–25] have made significant strides in the field of high-energy neutrino astrophysics [11, 26]. The groundbreaking discovery of a diffuse flux of high-energy neutrinos of astrophysical origin [16, 27, 28] heralded the birth of high-energy neutrino astronomy. High-energy astrophysical neutrinos in the TeV–PeV range and beyond are believed to be produced in the most extreme environments, such as active galactic nuclei, starburst galaxies, and gamma-ray bursts. This has been confirmed by the recent observation of the first candidate astrophysical high-energy neutrino sources, the blazar TXS 0506+056 [29, 30] and the Seyfert galaxy NGC 1068 [31].

High-energy neutrinos can shed light on the physical processes taking place in these extreme environments and help to answer fundamental questions about the nature of the Universe [14]. Yet, our understanding of the sources and mechanisms of high-energy astrophysical neutrino production remains incomplete.

In this context, flavor-composition measurements have emerged as an essential tool in the arsenal of high-energy neutrino astrophysics. Neutrinos exist in three flavors—electron (ν_e), muon (ν_μ), and tau (ν_τ). They are produced with a certain flavor composition at the sources and undergo flavor oscillations during their journey from the sources to the detector. Therefore, the flavor of a single neutrino tells us very little about its history, but the flavor composition of the ensemble of detected neutrinos—*i.e.*, the proportion of ν_e , ν_μ , and ν_τ in the diffuse neutrino flux that reaches Earth—carries crucial information about their production mechanisms, the identity of the neutrino sources, propagation effects, and even potential new physics [32–50].

So far, flavor-composition measurements have faced two main challenges: a limited number of detected neutrinos and the difficulty in identifying the flavor of individual neutrino events [18]. The interpretation of flavor measurements also suffers from uncertainties in the neutrino production and propagation. Thus, until now, such measurements have been done by averaging over a broad

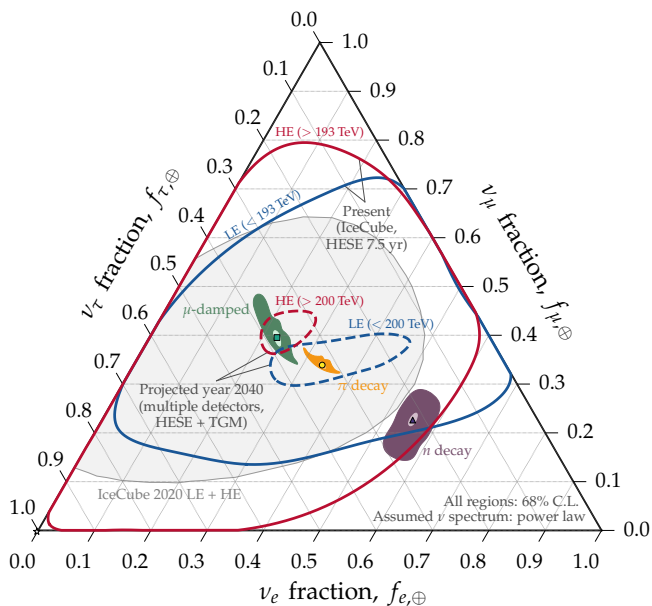


FIG. 1. *Present and projected measurements of the high-energy neutrino flavor composition at low (LE) and high energy (HE).* Measurements are of the flavor composition at Earth, $f_{\alpha,\oplus}^{\text{LE}}$ and $f_{\alpha,\oplus}^{\text{HE}}$ ($\alpha = e, \mu, \tau$). Present-day measurements are from the 7.5-year IceCube High-Energy Starting Event (HESE) sample [16, 17]. Projections for the year 2040 are from HESE plus TGM detected by multiple planned detectors (Table I). In this figure, the neutrino spectrum is assumed to be a power law in energy. For comparison, we show the previous energy-averaged measurement by IceCube (“IceCube 2020 LE + HE”) [18]. The allowed flavor regions for neutrino production via pion decay, muon-damped production, and neutron decay are computed as in Ref. [19], assuming present-day [20, 21] and projected [19] uncertainties in the neutrino mixing parameters. The regions shown are at 68% credibility level (C.L.). See Fig. 3 for other results and the main text for details. *Today, there is no evidence for a flavor transition in energy; by 2040, we could discover one.*

neutrino energy range [18, 38, 51].

However, it is unlikely that in reality the flavor composition is completely energy-independent, since we expect different neutrino production mechanisms, with different yields of ν_e , ν_μ , and ν_τ , to dominate at different energies. New physics effects could also modify flavor oscillations of neutrinos of different energies.

In this work, we go beyond prior analyses by considering the prospects and challenges of measuring the high-energy astrophysical neutrino flavor composition if it is different at different neutrino energies. To do this, we consider three general benchmark scenarios for the shape of the neutrino energy spectrum, which is currently still uncertain: a single power law, a broken power law, and an abrupt change in spectrum normalization, each associated with a flavor transition from a low-energy (LE) value to a high-energy (HE) value. We then examine the ability of neutrino telescopes to detect the existence of a flavor transition, measure the flavor composition at low

and high energy, and from that infer the flavor composition at the sources [19, 52].

To do this, we first use existing IceCube data, and then produce forecasts based on next-generation neutrino telescopes, either proposed or under construction [9, 10]: Baikal-GVD [53], IceCube-Gen2 [54], KM3NeT [55], P-ONE [56], TAMBO [57], and TRIDENT [58]. These telescopes will expand the cumulative rate of detection of high-energy neutrinos by over one order of magnitude. We present forecasts based on information that has been publicly presented by the above experimental collaborations, including expected detector operation timelines, but point out that experimental configurations and timing will undoubtedly change during detector development, compressing or expanding these timelines.

Figure 1 illustrates our results for the measurement of the flavor composition at Earth; later, Fig. 3 shows complete results. We find that, today, there is no evidence of a flavor transition in energy in the sample of High-Energy Starting Events (HESE) detected by IceCube over 7.5 years [16, 17]. However, our projections show sensitivity to detect a transition from pion decay at LE to muon-damped at HE in the coming years, using the combined detection of HESE and TGM events by the above upcoming neutrino telescopes. These observations hold regardless of our choice of the shape of the neutrino spectrum from among our benchmarks. Later, we show that this implies promising sensitivity to infer the flavor composition with which neutrinos are produced (Fig. 7).

Our results pave the way toward a richer understanding of astrophysical high-energy neutrino production and enhanced searches for new high-energy neutrino physics.

The rest of this article is organized as follows. In Section II we describe the distinct astrophysical scenarios considered in this work. In Section III we describe the different experiments involved in our global analysis. In Section IV we describe our analysis techniques. In Section V we show our results for the measurement of the flavor composition at Earth and at the sources. In Section VI we list envisioned improvements to our work. In Section VII we conclude.

II. ASTROPHYSICAL SCENARIOS

A. High-energy neutrino production

Although the identities of the astrophysical sources responsible for the bulk of high-energy neutrinos detected are so far unknown, they are presumably cosmic accelerators—likely predominantly extragalactic—capable of boosting cosmic-ray protons and nuclei to energies of at least a few tens of PeV [9, 59–61]. Upon interacting with matter [62–64] or radiation [63, 65–68], these protons produce intermediate particles that decay to yield high-energy neutrinos.

High-energy neutrinos are believed to be primarily produced in the decay of pions via $\pi^- \rightarrow \mu^- + \bar{\nu}_\mu$, followed by

$\mu^- \rightarrow e^- + \bar{\nu}_e + \nu_\mu$, and their charge-conjugated processes. These pions are produced via photohadronic or hadronuclear processes of high-energy CRs and each neutrino receives about 5% of the energy of the parent proton. Therefore, from the full pion decay chain, the expected flavor composition of the neutrinos just after leaving the sources (S) is $(f_{e,S} : f_{\mu,S} : f_{\tau,S}) = (1 : 2 : 0)$, where $f_{\alpha,S}$ ($\alpha = e, \mu, \tau$) is the ratio of $\nu_\alpha + \bar{\nu}_\alpha$ to the total flux. Below, we denote by ν_α the sum $\nu_\alpha + \bar{\nu}_\alpha$, unless otherwise indicated, since high-energy neutrino telescopes cannot presently distinguish between them.

The full pion decay chain yields the canonical expectation for the flavor composition of high-energy astrophysical neutrinos. However, there are alternatives. In sources that harbor intense magnetic fields, the intermediate muons might cool via synchrotron radiation before decaying. In this muon-damped case, the only high-energy neutrinos are the ν_μ produced directly in the decay of the pions, *i.e.*, $(0 : 1 : 0)_S$. In addition, neutrinos may be produced in the beta-decay of neutrons, $n \rightarrow p + e^- + \bar{\nu}_e$, which yields a pure- $\bar{\nu}_e$ flux, *i.e.*, $(1 : 0 : 0)_S$, though these neutrinos may be more relevant at lower energies.

Other flavor compositions at the sources are possible (see, *e.g.*, Refs. [36, 67]), but we adopt the three cases above—pion decay, muon-damped, and neutron decay—as benchmarks. Later we explore transitions with neutrino energy between the first two (Section II C).

B. Flavor composition at Earth

After the high-energy neutrinos leave their sources, they travel cosmological-scale distances en route to Earth. During that time, two effects modify the flavor content of their flux. First, neutrinos oscillate in flavor; owing to their high energies, the oscillations vary rapidly with energy. Second, the neutrino mass eigenstates, ν_1 , ν_2 , and ν_3 , whose superposition makes up the neutrino flavor states, separately. As a result, high-energy neutrinos arrive at Earth as an incoherent sum of mass eigenstates, each containing a fraction $|U_{\alpha i}|^2$ of each flavor ($i = 1, 2, 3$), where U is the Pontecorvo-Maki-Nakagawa-Sakata (PMNS) matrix, which depends on the mixing parameters θ_{12} , θ_{23} , θ_{13} , and δ_{CP} , whose values are measured in oscillation experiments (Table II).

Thus, for a given choice of the flavor composition at the sources, the flavor composition at Earth (\oplus) is [32]

$$f_{\alpha,\oplus} = \sum_{\beta} f_{\beta,S} \sum_i |U_{\alpha i}|^2 |U_{\beta i}|^2. \quad (1)$$

Even when the sum of mass eigenstates is not fully incoherent, the limited energy resolution of the neutrino detector makes it difficult to resolve the rapid energy dependence of the flavor oscillations, which leads again to Eq. (1) being the measurable flavor composition at Earth in practice. New physics that modifies the flavor composition at Earth effectively modifies Eq. (1). Rather

than exploring these deviations for specific new-physics models, later we explore classes of models generically by proxy, using benchmark neutrino spectra that include flavor transitions and that capture those deviations (Section II D). In all cases, we adopt Eq. (1) in our analysis below to compute the flavor composition at Earth.

We provide context for our measurements of the flavor composition by contrasting them against the allowed regions of flavor composition at Earth for our three benchmark choices of flavor composition at the sources (Section II A) and, also, for any combination of flavor composition at the sources (Figs. 1 and 3).

We generate the allowed regions as in Ref. [19] (see also Ref. [36]), via FANFIC [69]. To generate the present-day allowed flavor regions, we use the present-day values of the mixing parameters from the recent NuFIT 5.1 [20, 21] global fit to oscillation data (Table II). Evaluating the mixing parameters at their present-day best-fit values yields $(0.33 : 0.34 : 0.33)_\oplus$ for neutrino production via the full pion decay chain, $(0.23 : 0.39 : 0.38)_\oplus$ for muon-damped production, and $(0.55 : 0.23 : 0.22)_\oplus$ for production via neutron decay. The present-day allowed regions of flavor composition at Earth—the *theoretically palatable region* [36]—are already relatively narrow, their sizes spanned mainly by the uncertainty in θ_{12} and θ_{23} .

By 2040, we expect the allowed flavor regions at Earth to shrink dramatically (Figs. 1 and 3), due to the foreseen improvement [19] in precision in the measurement of the mixing parameters by upcoming experiments DUNE [70], Hyper-Kamiokande [71], and JUNO [72]. Table II shows that by 2040 $\sin^2\theta_{23}$ and $\sin^2\theta_{12}$ will be constrained to within 1% precision, and that the correlation between $\sin^2\theta_{23}$ and δ_{CP} that exists today [20] will vanish.

Later, in Section IV B, we use the present and projected distributions of the mixing parameters also to infer the flavor composition at the neutrino sources.

C. Low-to-high-energy flavor transitions

In general, the flavor composition might be different at different neutrino energies. This could be due to effects from astrophysics—*i.e.*, the dominant neutrino production mechanism changing with energy—or from neutrino physics—*i.e.*, neutrino oscillations being affected by non-standard effects. We survey these possibilities below.

Regarding astrophysics, a transition from pion-decay to muon-damped flavor composition from low to high neutrino energies could occur if the diffuse flux is due to a class of neutrino sources that harbor intense magnetic fields; see, *e.g.*, Refs. [73–78]. The magnetic field intensity in the sources determines the energy at which the flavor transition occurs, *i.e.*, at which intermediate muons cool significantly via synchrotron radiation. A related possibility is that the diffuse flux originates from two different source populations, each emitting neutrinos with a different flavor composition and dominating in different energy ranges [79, 80].

Regarding neutrino physics, there is a large number of effects that could act during neutrino production, propagation, and detection to modify the flavor composition in an energy-dependent manner [41]. During propagation alone, examples include neutrino decay [36, 40, 81–87], Lorentz invariance violation [37, 50, 88–91], dark matter interactions [43, 92, 93], non-standard interactions [45, 84, 94–96], sterile neutrinos [39, 46–48], pseudo-Dirac neutrinos [49, 84, 97, 98], renormalization group-running of the neutrino mixing parameters [99], and the violation of the equivalence principle [42, 100–103].

To assess the capability of identifying a flavor transition, we adopt a generic form of it that captures the essence of the transitions in the above models, rather than modeling each model separately. We assume that the flavor composition of the observed diffuse neutrino flux transitions from a LE value, $(f_{e,\oplus}^{\text{LE}}, f_{\mu,\oplus}^{\text{LE}}, f_{\tau,\oplus}^{\text{LE}})$, to a HE value, $(f_{e,\oplus}^{\text{HE}}, f_{\mu,\oplus}^{\text{HE}}, f_{\tau,\oplus}^{\text{HE}})$, at an energy E_{trans} .

Later, in Sections IV and V, when analyzing present data, we make no assumptions on the values of these parameters, but rather extract them from the data. When making projections, we assume that the flavor composition transitions from pion decay at LE to muon-damped at HE (see Section II B for the numerical values) and that $E_{\text{trans}} = 200$ TeV or 1 PeV, and we assess how well we can recover those values from mock projected data.

Our choice of looking for a transition between the flavor composition from pion decay to that from muon-damped pion decay is conservative, since under standard oscillations they are fairly close to each other and, therefore, are challenging to distinguish; see Figs. 1 and 3. In contrast, particular new-physics effects may introduce large deviations in the flavor composition relative to both of these benchmarks, making them easier to identify.

Often, changes to the flavor composition are accompanied by changes to the neutrino energy spectrum; next, we account for this.

D. Neutrino energy spectrum

Figure 2 shows the three benchmark choices of the neutrino spectrum that we adopt in our analysis, illustrated for $E_{\text{trans}} = 1$ PeV. At that energy, the flavor composition transitions (see Section II C). For one of our benchmarks (PL below), this is the only change that occurs; for the remaining two (BPL and Step below), the flavor transition is accompanied by a transition in the shape of the all-flavor spectrum.

Single power law spectrum (PL): This is our barest prescription: a power law in neutrino energy, $\Phi_\nu \propto E_\nu^{-\gamma}$, with a spectral index γ common to all flavors, and with an abrupt flavor transition at energy E_{trans} , but no change in the energy spectrum. This spectrum may mimic, *e.g.*, the transition due to neutrino decay or Lorentz invariance violation, in which the energy spectrum is not necessarily af-

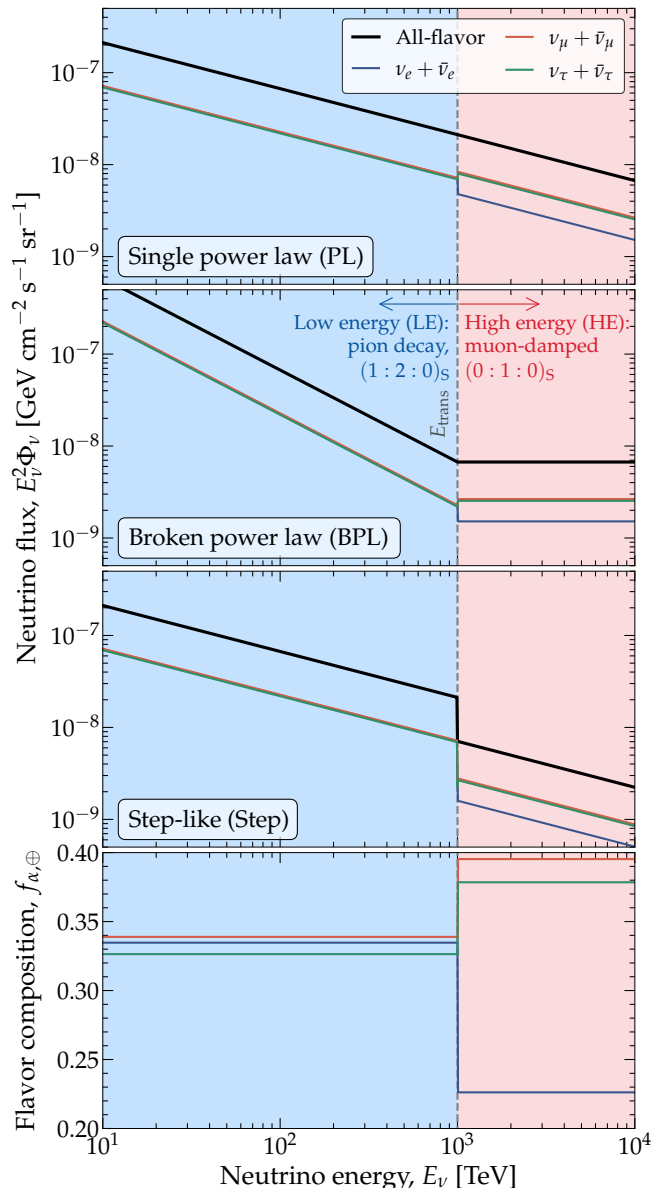


FIG. 2. *Benchmark models of the high-energy neutrino spectrum at Earth.* The flavor composition, $f_{\alpha,\oplus}$, transitions at the energy E_{trans} from that expected from production via the full pion decay chain at LE to that expected from muon-damped production at HE. For this plot, we compute the fluxes using the benchmark true values in Table II and set $E_{\text{trans}} = 1$ PeV; in our results, we consider also 200 TeV. *Top panels:* Neutrino spectra. *Bottom panel:* Flavor composition at Earth, common to the three benchmark spectra. See Section II for details. *Our benchmark spectra capture the main features of a large variety of predicted changes to the flavor composition with energy.*

ected by the onset of new-physics effects that alter the flavor composition.

Broken power law spectrum (BPL): The spectrum is a power law that changes slope at the flavor tran-

sition, *i.e.*, it is $\propto E_\nu^{-\gamma^{\text{LE}}}$ below E_{trans} and $\propto E_\nu^{-\gamma^{\text{HE}}}$ above it. This spectrum may mimic, *e.g.*, a scenario where the LE flux is dominated by sources that emit neutrinos with a steep energy spectrum, like NGC 1068 [31], and the HE flux, by sources that emit neutrinos with a shallow energy spectrum, like TXS 0506+056 [29, 30].

Step-like spectrum (Step): The spectrum is a power law $\propto E^{-\gamma}$, whose all-flavor normalization has a step-like, abrupt change at the flavor transition. This spectrum roughly approximates a more realistic transition between the pion-decay and muon-damped flavor compositions. Since, in the latter, only the neutrinos from the direct pion decay, which comprise one third of the total, have high energies, the flavor transition is accompanied by a factor-of-3 reduction in the flux.

In our benchmark spectra above, the flavor transition is abrupt in energy. In reality, the transition may be softer due to the distribution of the sources in redshift—which smears the energy spectrum with which neutrinos are emitted—or to the spread in the values of the parameters that affect neutrino production within the population of neutrino sources; *e.g.*, Refs. [67, 75]. However, limited energy resolution and event rates render detectors largely insensitive to the detailed dependence of the flavor transition with energy. Hence, our choice of an abrupt transition, although possibly unrealistic, should not affect our results significantly.

Later, as part of our statistical analysis in Section IV, we vary the values of the parameters that dictate the spectrum shape and the flavor composition below and above the transition, generate mock samples of detected events, and contrast them to samples generated using the assumed true values of the parameters. Table II shows the free model parameters that we vary in our analysis; we defer further discussion to Section IV.

III. PRESENT AND NEAR-FUTURE NEUTRINO TELESCOPES

A. High-energy neutrino telescopes

We focus on mainly optical “plum pudding”-style neutrino telescopes, consisting of a large volume of natural water or ice, instrumented with strings of photomultiplier tubes (PMTs) designed to detect the Cherenkov light emitted primarily by the electromagnetic products of neutrino-nucleon deep-inelastic scattering (DIS) [104–107]. Depending on detector size and string spacing, these can be effective from neutrino energies of a few GeV to upward of 10–100 PeV. (Above these energies, alternative detection strategies, such as in-ice Askaryan radio-detection, are more suitable [9, 108].)

To produce our results, we use present-day data from IceCube, and projections for the planned

TABLE I. *High-energy neutrino telescopes considered in this work.* The detector sizes are given in units of the size of IceCube (IC), which is approximately 1 km³. This factor rescales the expected rates of IceCube HESE events, computed using the IceCube Monte Carlo sample, and of IceCube TGM events. The start and end years are estimated. For IceCube, the start year is for the final detector configuration (we do not account for detection during detector construction) and the end year is when IceCube-Gen2 is estimated to start operations. See Section III A for details.

Detector	Size relative to IceCube	Start year	End year
IceCube	1 IC	2011	2030
Baikal-GVD	1.5 IC	2025	...
KM3NeT	2.8 IC	2025	...
IceCube-Gen2	8 IC	2030	...
P-ONE	3.2 IC	2030	...
TAMBO	0.5 IC	2030	...
TRIDENT	7.5 IC	2030	...

optical-Cherenkov telescopes Baikal-GVD, IceCube-Gen2, KM3NeT, P-ONE, and TRIDENT. Additionally, we consider TAMBO, a surface array of water-Cherenkov detectors that targets PeV-scale ν_τ . We do not consider the recent proposal for a 30-km³ in-water Cherenkov detector [109, 110], since it is still preliminary.

A core assumption in making our predictions is that the capabilities of future detectors to detect HESE and TGM will be comparable to those of IceCube. Neutrino detection at IceCube serves as the basis of our projections for detection in upcoming telescopes: as in Refs. [19, 50, 111, 112], we estimate neutrino detection in each future telescope by scaling the rate of detected events in IceCube (Section III B) by the size of the detector relative to IceCube (Table I). Admittedly, this is a crude approximation that foregoes detailed modeling of the specific capabilities of upcoming detectors, made necessary by the present lack of publicly available simulations of the performance of upcoming telescopes to the same level of detail as it is available for IceCube.

Table I summarizes our assumptions about the size and dates of operation of the detectors, both of which are based on current estimates and subject to change in the future. For future detectors, we consider data-taking only after they reach their final sizes, which yields conservative results, since detection during their construction phases would add additional data.

IceCube: The IceCube Neutrino Observatory, at the South Pole, has been operational for over ten years. It consists of a cubic kilometer of clear ice with 86 vertical strings, each equipped with 60 optical modules that house PMTs to detect the Cherenkov light emitted by particle showers triggered by neutrino DIS [113]. Section III B describes the types

of events detected by IceCube that we use in our analysis—HESE and TGM—and how we model neutrino detection inasmuch detail as possible outside the Collaboration.

IceCube-Gen2: IceCube-Gen2 is the planned extension of IceCube [54, 114]. It will expand the detector by adding 120 new PMT strings, resulting in an instrumented volume of 7.9 km^3 , yielding an effective area that is 7 to 8.5 times larger than IceCube between 100 TeV and 1 PeV. The deployment of IceCube-Gen2 is scheduled to start in 2027 and aims for completion by 2033.

KM3NeT: KM3Net [55], the successor to ANTARES [25], is an in-water Cherenkov detector under construction in the Mediterranean Sea. It is split into two sites, one densely-instrumented low-energy site, ORCA, and a larger and sparser site optimized for higher energies, ARCA; we consider only the latter in our analysis (heretofore, we refer to it simply as KM3NeT). ARCA will consist of two clusters of 115 strings, each equipped with 18 optical modules per string, situated 100 km off the coast of Sicily. The construction is underway and is expected to be finalized by 2027. With an estimated event rate of 15.6 cascades (Section III B) induced by cosmic neutrinos per year, KM3Net is projected to have an event rate approximately 2.8 times that of IceCube. We adopt this as a benchmark, but the exact figure depends on the shape of the astrophysical neutrino energy spectrum.

Baikal-GVD: Baikal-GVD [115], in Lake Baikal, Siberia, the successor to the Baikal detector [23], is an in-water Cherenkov detector, in operation since 2018. Its current effective volume is 0.35 km^3 ; by 2025, when its construction is completed, it will reach 1.5 km^3 . Baikal-GVD consists of 90 strings, each equipped with 12 optical modules. It has already observed [116], tentatively, neutrinos from the blazar TXS 0506+056 previously observed by IceCube [29, 30] and the diffuse flux of high-energy astrophysical neutrinos [117].

P-ONE: P-ONE, the Pacific Ocean Neutrino Experiment [118], is a planned in-water Cherenkov experiment to be located off Vancouver Island in the Cascadia basin. By 2023, a first string has been deployed and six strings are funded and are under construction. The final configuration of P-ONE is expected to be completed by 2030 and will comprise 70 PMT strings, each equipped with 20 optical modules, covering a cylindrical volume with a height of 1 km and a radius of 1 km.

TRIDENT: TRIDENT [58], the Tropical Deep-Sea Neutrino Telescope, is a proposed in-water Cherenkov telescope to be located in the South

China Sea. The planned final configuration of TRIDENT consists of 1211 PMT strings yielding an effective volume of 7.5 km^3 , TRIDENT aims to begin construction in 2026 and reach its full size by 2030.

TAMBO: TAMBO [57, 119], the Tau Air-Shower Mountain-Based Observatory, is a proposed surface array of water-Cherenkov detectors designed to detect PeV-scale ν_τ via the upward-going tau showers they trigger, with an expected event rate of 7 ν_τ per year. Even though TAMBO is small compared to IceCube (Table I), its particular sensitivity to ν_τ provides unique, complementary information to plum-pudding-style optical neutrino telescopes, which are more evenly sensitive to all neutrino flavors. We assume a start date of TAMBO of 2030. We include the contribution of TAMBO by considering only one third of its proposed volume from Table I, to account for it being sensitive only to ν_τ . Since the neutrino detection strategy of TAMBO is different from the other neutrino telescopes discussed in this work, modeling it as a scaled-down version of IceCube is a particularly coarse approximation, but given its relative size the effect of mis-modeling it on our results is small.

B. Types of detected events

High-energy neutrino telescopes detect neutrinos primarily via neutrino deep-inelastic scattering (DIS) on nucleons, N . A DIS interaction can be either charged-current (CC), *i.e.*, $\nu_\alpha + N \rightarrow l_\alpha + X$, with X final-state hadrons, or neutral-current (NC), *i.e.*, $\nu_\alpha + N \rightarrow \nu_\alpha + X$. At these energies, the DIS cross sections of ν_α and $\bar{\nu}_\alpha$ are nearly equal, and we do not distinguish between events made by one or the other. The final-state hadrons receive, on average, 20% of the energy the initial-state neutrino; the final-state lepton receives the rest.

Charged final-state particles initiate high-energy showers; as they develop, they emit Cherenkov light that propagates through the ice and is detected by the PMTs. From the spatial and temporal distribution of the detected light, *i.e.*, from the *event morphology*, analyses infer the energy and direction of the interacting neutrino. From the relative number of events with different morphologies, analyses infer the flavor composition of the incoming flux of neutrinos.

To measure the flavor composition, we use two classes of detected events in high-energy neutrino telescopes: HESE—made by neutrinos of all flavors—and TGM—made mainly by ν_μ .

1. High-Energy Starting Events (HESE)

HESE events are triggered by the interaction of neutrinos inside the instrumented detector volume. Differ-

ent neutrino flavors interacting via CC and NC generate three distinct HESE event morphologies: cascades, tracks, and double cascades. The flavor composition of the neutrino flux responsible for a sample of detected HESE events is inferred by comparing the numbers of detected events of each morphology.

Cascades: Cascades are generated primarily by the CC interaction of ν_e . In one such interaction, the showers initiated by the final-state electrons and hadrons are superimposed and treated as one. Cascades are also generated by the CC interaction of ν_τ that produce short-lived final-state tau leptons whose decay length is shorter than the spacing between detector modules, such that the shower it initiates is indistinguishable from that initiated by the hadrons. Finally, cascades are also generated by NC interactions of ν_e , ν_μ , and ν_τ . At a given energy, the NC contribution is subdominant because the NC cross section is smaller than the CC cross section and NC interactions deposit less energy into the shower, since only the final-state hadrons shower, though this is partially compensated by the fact that all flavors contribute.

Tracks: Tracks are generated by the CC interaction of ν_μ and by the 17% of CC interactions of ν_τ that produce a final-state muon [120]. In both cases, energetic muons propagate over tens of kilometers while losing energy, leaving tracks of Cherenkov light that are easily identifiable.

Double cascades: Double cascades are generated by the CC interaction of energetic ν_τ [32]. A first cascade initiated by the final-state hadrons is followed by a second cascade initiated by the hadronic decay of the final-state tau lepton. Double cascades are identifiable for ν_τ that are sufficiently energetic to yield final-state tau leptons whose decay length exceeds the spacing between detector modules. Recently, IceCube observed the first two candidate double cascades [18]. The requirement of needing to observe the two cascades makes double cascades rare in the sample of detected events, but because they are clean evidence of ν_τ they improve the measurement of the flavor composition appreciably [18].

The contribution of neutrino-electron interactions to the event rate is ordinarily negligible, except within a narrow energy range around the Glashow resonance [121] at $E_\nu = 6.3$ PeV. There, the scattering of $\bar{\nu}_e$ on electrons is enhanced significantly by the production of an on-shell W boson. Recently, IceCube detected the first candidate Glashow resonance event [122]. Detecting the Glashow resonance could allow us to break the degeneracy between events due to ν_e and $\bar{\nu}_e$ [86, 112, 123–125].

The description of the event morphologies above exposes the core challenge in measuring the flavor composition: cascades and tracks can be made by more than

one neutrino flavor, so it is not possible to firmly infer the flavor of any individual detected event. This is aggravated by the limited energy and angular resolution of the detector, and by the fact that morphologies are occasionally mis-identified [35, 126].

We account for these nuances by basing our computation of HESE event rates on the publicly available IceCube Monte Carlo (MC) sample of HESE events [17], released together with 7.5 year HESE sample [16]. With it we compute separately the rates of HESE cascades—including from the Glashow resonance—tracks, and double cascades. The MC sample accounts for the attenuation of the neutrino flux due to neutrino interactions with matter as it propagates inside the Earth, and implicitly contains a detailed description of IceCube, including of the relation between different flavors and morphologies. We defer to Refs. [16, 17] and present a short overview in Section IV.

2. Through-going muons (TGM)

A muon of energy larger than TeV can travel hundreds to thousands of meters, eventually crossing the neutrino detector and leaving an identifiable track of Cherenkov light in its wake. The interacting muon can be of atmospheric origin, created in cosmic-ray-induced air showers, or it can be created in a ν_μ CC interaction in the ice. In the latter case, the long travel range of high-energy muons means that tracks can be detected even if the neutrino interactions that birth them happen far away, thus effectively extending the size of the detector.

In our analysis, we consider TGM, an event sample made up of tracks induced by CC interactions of ν_μ outside the detector. In TGM samples, cascade-like events are filtered out. To circumvent the overwhelming background of atmospheric muons, our TGM samples are limited to up-going events, *i.e.*, events that reach the detector from below it. As a result, in our samples, up-going atmospheric muons are stopped inside Earth before reaching the detector, leading to a neutrino purity larger than 99.8% [127].

Including TGM events in our analysis vastly increases the number of events. For comparison, IceCube detected 650,000 TGM events in 9.5 years [127] *vs.* 102 HESE events in 7.5 years [16], with the caveat that most TGM events out of those are of atmospheric origin. We combine TGM only in our projections, as explained below. For the measurement of the flavor composition, including TGM events improves the measurement precision of the ν_μ fraction; we show this explicitly in Section V A.

Unlike our HESE track samples, in our TGM samples we only include the contribution from muons made by ν_μ , not by ν_τ , since this is a recent development in the point-source searches that we base our samples off of.

3. Combining HESE and TGM events

By themselves, HESE events provide sensitivity to the flavor composition. In our present-day results, we use HESE events exclusively. However, their paucity limits the precision of the flavor-composition measurement.

To address this, in our projections we combine HESE events with TGM. Our strategy is similar to Refs. [51, 128], which, however, measured the flavor composition assuming that it is constant in energy. Because vastly more TGM are detected than HESE events, combining them tightens the measurement of the muon-flavor content significantly.

IV. METHODS

Within our benchmark flux scenarios (Section II), we look for the presence of a flavor transition as a function of neutrino energy using present IceCube observations and mock projected observations by upcoming neutrino telescopes (Section III). For present data, we use the publicly available 7.5-year sample of IceCube HESE events [16, 17]. For projections, we simulate data with two distinct event selections, HESE and TGM, based on the PLE ν M framework [129], and perform our analysis with them combined. Our statistical methods are Bayesian. We perform two main tasks: measuring the flavor composition at Earth and, based on it, inferring the flavor composition at the neutrino sources.

A. Measuring the flavor composition at Earth

For a given choice of spectrum shape from among our benchmarks (Section IID), our goal is to measure the flavor composition at Earth at low and high energy, $f_{\alpha,\oplus}^{\text{LE}}$ and $f_{\alpha,\oplus}^{\text{HE}}$, respectively. We do so by contrasting samples of observed events, real or mock, against test event samples computed under different assumptions of spectrum shape and flavor composition, in search for the ones that describe the observations best.

Table II shows the free model parameters that we vary in our analysis, and the prior distributions that we use for them later in our statistical analysis. Which spectrum shape parameters are varied depends on our choice of spectrum shape from our PL, BPL, and Step benchmarks. The flavor composition at LE, given by $f_{e,\oplus}^{\text{LE}}$ and $f_{\mu,\oplus}^{\text{LE}}$, is varied independently from the flavor composition at HE, $f_{e,\oplus}^{\text{HE}}$ and $f_{\mu,\oplus}^{\text{HE}}$. (Because $\sum_{\alpha} f_{\alpha,\oplus}^{\text{LE}} = \sum_{\alpha} f_{\alpha,\oplus}^{\text{HE}} = 1$, we only need vary the electron and muon flavor content.)

To ensure that the flavor fractions are sampled uniformly as part of our statistical analysis, we parametrize them as $(f_{e,\oplus}^{\text{LE}}, f_{\mu,\oplus}^{\text{LE}}, f_{\tau,\oplus}^{\text{LE}}) \equiv (\sin^2 \theta_{\oplus}^{\text{LE}} \cos^2 \psi_{\oplus}^{\text{LE}}, \sin^2 \theta_{\oplus}^{\text{LE}} \sin^2 \psi_{\oplus}^{\text{LE}}, \cos^2 \theta_{\oplus}^{\text{LE}})$, where $\theta_{\oplus}^{\text{LE}}$ and $\psi_{\oplus}^{\text{LE}}$ are ancillary angles, and similarly for HE. Then we build priors based on

the Haar measure [130] of the volume element $df_{e,\oplus}^{\text{LE}} \wedge df_{\mu,\oplus}^{\text{LE}} \wedge df_{\tau,\oplus}^{\text{LE}} = d(\sin^4 \theta_{\oplus}^{\text{LE}}) \wedge d(\cos 2\psi_{\oplus}^{\text{LE}})$. By using uniform priors to sample $\sin^4 \theta_{\oplus}^{\text{LE}} \in [0, 1]$ and $\cos 2\psi_{\oplus}^{\text{LE}} \in [-1, 1]$, and similarly for HE, we ensure an unbiased sampling of the flavor fractions.

In describing our statistical methods below, we collect the spectrum shape parameters and flavor-composition parameters into the parameter set Θ_{\oplus} , whose contents depend on the choice of benchmark flux:

Single power law spectrum (PL):

$$\Theta_{\oplus}^{\text{PL}} = (\Phi_{\nu,0}, \gamma, \sin^4 \theta_{\oplus}^{\text{LE}}, \cos 2\psi_{\oplus}^{\text{LE}}, \sin^4 \theta_{\oplus}^{\text{HE}}, \cos 2\psi_{\oplus}^{\text{HE}}, E_{\text{trans}}) \quad (2)$$

Broken power law spectrum (BPL):

$$\Theta_{\oplus}^{\text{BPL}} = (\Phi_{\nu,0}^{\text{LE}}, \Phi_{\nu,0}^{\text{HE}}, \gamma, \sin^4 \theta_{\oplus}^{\text{LE}}, \cos 2\psi_{\oplus}^{\text{LE}}, \sin^4 \theta_{\oplus}^{\text{HE}}, \cos 2\psi_{\oplus}^{\text{HE}}, E_{\text{trans}}) \quad (3)$$

Step-like spectrum (Step):

$$\Theta_{\oplus}^{\text{Step}} = (\Phi_{\nu,0}, \gamma^{\text{LE}}, \gamma^{\text{HE}}, \sin^4 \theta_{\oplus}^{\text{LE}}, \cos 2\psi_{\oplus}^{\text{LE}}, \sin^4 \theta_{\oplus}^{\text{HE}}, \cos 2\psi_{\oplus}^{\text{HE}}, E_{\text{trans}}) \quad (4)$$

Table II summarizes the above parameter sets.

B. Inferring the flavor composition at the sources

Using the methods introduced in Ref. [52] (see also Ref. [19]), we can infer the flavor composition at the neutrino sources. The process involves undoing the effect of flavor oscillations during neutrino propagation to Earth, given the flavor composition measured at Earth and knowledge of the allowed ranges of the neutrino mixing parameters. For the first time, we do this separately at low and high energy, *i.e.*, we infer $f_{\alpha,S}^{\text{LE}}$ and $f_{\alpha,S}^{\text{HE}}$. Because we use the diffuse neutrino flux, made up of the contributions from the full population of neutrino sources, what we infer is the population-averaged flavor composition at the sources.

Table II show the free parameters and priors that we vary in our statistical analysis. Because standard scenarios of high-energy astrophysical neutrino production do not yield ν_{τ} , when inferring the flavor composition at the sources we assume $f_{\tau,S}^{\text{LE}} = f_{\tau,S}^{\text{HE}} = 0$ and so we need only infer the electron flavor fraction at LE, $f_{e,S}^{\text{LE}}$, and at HE, $f_{e,S}^{\text{HE}}$. For the neutrino mixing parameters, under the requirement of Haar measure, we choose parameters $\Omega = (\sin^2 \theta_{12}, \cos^4 \theta_{13}, \sin^2 \theta_{23}, \delta_{\text{CP}})$, and use the same present-day and projected probability distributions (Table II) that we use to compute the allowed flavor regions at Earth in Figs. 1 and 3.

In describing our statistical methods below, we collect the spectrum shape parameters and flavor-composition parameters into the parameter set Θ_S , whose contents depend on the choice of benchmark flux:

TABLE II. *Free model parameters considered in this work.* The spectrum shape parameters define the neutrino energy spectrum in our three benchmark flux models (Fig. 2): single power law (PL), broken power law (BPL), and step-like (Step). The transition from a pion-decay flavor composition at LE to a muon-damped flavor composition at HE takes place at neutrino energy E_{trans} . In our statistical analysis, the parameter values are varied as within the ranges given in the table. See Section II for details on the flux models. See Section IV A for details on the parametrization of the flavor composition at Earth used when inferring the flavor composition at the sources.

Parameter	Symbol	Units	Used in flux model			True value (in proj.) ^a	Prior
			PL	BPL	Step		
Spectrum shape parameters (Section II D)							
All-flavor flux normalization at 100 TeV, common to LE and HE	$\Phi_{\nu,0}$	$10^{-18} \text{ GeV}^{-1} \text{ cm}^{-2} \text{ s}^{-1} \text{ sr}^{-1}$	✓	✓		6.7	Uniform $\in [0, 10]$
LE all-flavor flux normalization at 100 TeV	$\Phi_{\nu,0}^{\text{LE}}$	$10^{-18} \text{ GeV}^{-1} \text{ cm}^{-2} \text{ s}^{-1} \text{ sr}^{-1}$			✓	6.7	Uniform $\in [0, 10]$
HE all-flavor flux normalization at 100 TeV	$\Phi_{\nu,0}^{\text{HE}}$	$10^{-18} \text{ GeV}^{-1} \text{ cm}^{-2} \text{ s}^{-1} \text{ sr}^{-1}$			✓	(6.7/3)	Uniform $\in [0, 10]$
Energy of flavor transition, LE to HE	E_{trans}	TeV	✓	✓	✓	200 or 10^3	Log ₁₀ -uniform $\in [60, 10^4]$
Spectral index, common to LE and HE	γ	...	✓		✓	2.5	Uniform $\in [1, 4]$
LE spectral index	γ^{LE}	...		✓		3.0	Uniform $\in [1, 4]$
HE spectral index	γ^{HE}	...		✓		2.0	Uniform $\in [1, 4]$
Additional parameters used when measuring the flavor composition at Earth (Section IV A)							
LE angle of flavor composition at Earth	$\sin^4 \theta_{\oplus}^{\text{LE}}$...	✓	✓	✓	0.45	Uniform $\in [0, 1]$
LE angle of flavor composition at Earth	$\cos 2\psi_{\oplus}^{\text{LE}}$...	✓	✓	✓	-0.01	Uniform $\in [-1, 1]$
HE angle of flavor composition at Earth	$\sin^4 \theta_{\oplus}^{\text{HE}}$...	✓	✓	✓	0.39	Uniform $\in [0, 1]$
HE angle of flavor composition at Earth	$\cos 2\psi_{\oplus}^{\text{HE}}$...	✓	✓	✓	-0.27	Uniform $\in [-1, 1]$
Additional parameters used when inferring the flavor composition at the sources (Section IV B)							
LE electron flavor fraction	$f_{e,\oplus}^{\text{LE}}$...	✓	✓	✓	0.33	Uniform $\in [0, 1]$
HE electron flavor fraction	$f_{e,\oplus}^{\text{HE}}$...	✓	✓	✓	0.23	Uniform $\in [0, 1]$
Solar mixing angle	$\sin^2 \theta_{12}$...	✓	✓	✓	0.304	Present ^b : 0.304 ± 0.012 Proj. ^c : Normal, $\sigma = 0.002$
Atmospheric	$\sin^2 \theta_{23}$...	✓	✓	✓	0.450	Present ^b : $0.450^{+0.016}_{-0.019}$ Proj. ^c : Normal, $\sigma = 0.004$
Reactor mixing angle	$\sin^2 \theta_{13}$...	✓	✓	✓	0.304	Present ^b : 0.02246 ± 0.00062 Proj. ^c : Normal, $\sigma = 0.00062$
CP-violation phase	δ_{CP}	°	✓	✓	✓	230	Present ^b : 230^{+25}_{-36} Proj. ^c : Normal, $\sigma = 6.687$

^a The true parameters values are used only when making projections, to generate mock samples of observed events.

^b We build the present-day likelihood of the mixing parameters from the $\Delta\chi^2$ distributions of the NuFit 5.1 global fit to oscillation data. We treat $\sin^2 \theta_{12}$ and $\sin^2 \theta_{13}$ as uncorrelated with the others, and $\sin^2 \theta_{23}$ and δ_{CP} as correlated between them via a two-dimensional joint likelihood. In the table, for brevity, we show only the approximate one-dimensional 68% credible intervals, but our results are generated using the detailed shape of the NuFIT distributions.

^c All of the year-2040 projected likelihoods of the mixing parameters are one-dimensional normal distributions centered at their present-day best-fit values from NuFIT 5.1, with standard deviation σ . There is no correlation between parameters; see Ref. [19]. The projected uncertainties shown in the table apply to the normal and inverted neutrino mass ordering.

Single power law spectrum (PL):

$$\Theta_{\text{S}}^{\text{PL}} = (\Phi_{\nu,0}, \gamma, f_{e,\text{S}}^{\text{LE}}, f_{e,\text{S}}^{\text{HE}}, E_{\text{trans}}) \cup \Omega \quad (5)$$

Broken power law spectrum (BPL):

$$\Theta_{\text{S}}^{\text{BPL}} = (\Phi_{\nu,0}^{\text{LE}}, \Phi_{\nu,0}^{\text{HE}}, \gamma, f_{e,\text{S}}^{\text{LE}}, f_{e,\text{S}}^{\text{HE}}, E_{\text{trans}}) \cup \Omega \quad (6)$$

Step-like spectrum (Step):

$$\Theta_{\text{S}}^{\text{Step}} = (\Phi_{\nu,0}, \gamma^{\text{LE}}, \gamma^{\text{HE}}, f_{e,\text{S}}^{\text{LE}}, f_{e,\text{S}}^{\text{HE}}, E_{\text{trans}}) \cup \Omega \quad (7)$$

Table II summarizes the above parameter sets.

C. HESE likelihood

The HESE MC sample [17] provides, for each simulated event, primary quantities, *i.e.*, neutrino energy, zenith angle, and flavor, and reconstructed quantities, *i.e.*, deposited energy, reconstructed zenith angle, morphology—cascade (c), track (tr), or double cascade (dc)—and, for double cascades, reconstructed track length. As in the analysis of the 7.5-year HESE sample by the IceCube Collaboration [16], we use HESE events detected with energies above 60 TeV.

In searches for astrophysical neutrinos, the background is due to atmospheric muons and neutrinos. In our analysis, we fix their fluxes to their best-fit values found by IceCube, in Table VI.1 of Ref. [16]. Since the atmospheric contribution is subdominant above 60 TeV and negligible

above 100 TeV, this choice does not significantly impacts our results. We also fix the parameters governing detector systematic uncertainties, including the light acceptance of the optical module and ice properties, to their best-fit values reported in Ref. [16].

In the MC sample, the j -th event has an associated weight w_j that depends only on Θ_{\oplus} when measuring the flavor composition at Earth (Section IV A), or only on Θ_S when inferring the flavor composition at the sources (Section IV B). The weights allow us transform the HESE MC sample and generate Asimov event samples for different choices of the spectrum and flavor composition of the astrophysical neutrinos. For cascades and tracks, we compute the number of events in bins of deposited energy and reconstructed zenith angle; for double cascades, we compute it in bins of deposited energy and track length. We use the same binning scheme as in the IceCube HESE analysis, from Table V.1 of Ref. [16].

Using the weights, we compute the expected number of events of each morphology, $m = \{c, tr, dc\}$, due to

astrophysical neutrinos. In the i -th bin, this is

$$\mu_{m,i}^{\text{ast}}(\Theta) = \sum_{j \in \text{bin } i} w_{m,j}(\Theta), \quad (8)$$

where the sum is over the events that fall in that bin. The total number of expected events, $\mu_{m,i}$, includes also the contribution from atmospheric backgrounds, $\mu_{m,i}^{\text{atm}}$, *i.e.*,

$$\mu_{m,i}(\Theta) = \mu_{m,i}^{\text{ast}}(\Theta) + \mu_{m,i}^{\text{atm}}. \quad (9)$$

We also compute the expected variance,

$$\sigma_{m,i}^2(\Theta) = \sum_{j \in \text{bin } i} w_{m,j}^2(\Theta) + (\mu_{m,i}^{\text{atm}})^2, \quad (10)$$

to account for statistical fluctuations in event rate.

The expected event numbers and fluctuations are then compared against a sample of observed events, real for present-day data and mock for projections, which contains $N_{m,i}$ events of morphology m in the i -th bin. For present-day results, we use the IceCube 7.5-year HESE sample [16, 17]. For projections, we use Asimov data samples built with the mean expected rate, Eq. (9), *i.e.*, $N_{m,i} = \mu_{m,i}$. The comparison is performed using the same effective likelihood function used by the IceCube Collaboration in Ref. [16], *i.e.*,

$$\mathcal{L}_{\text{HESE}}(\Theta) = \prod_m^{\{c, tr, dc\}} \prod_i^{\text{bins}} \left(\frac{\mu_{m,i}}{\sigma_{m,i}^2} \right)^{\frac{\mu_{m,i}^2}{\sigma_{m,i}^2} + 1} \Gamma \left(N_{m,i} + \frac{\mu_{m,i}^2}{\sigma_{m,i}^2} + 1 \right) \left[N_{m,i}! \left(1 + \frac{\mu_{m,i}}{\sigma_{m,i}^2} \right)^{N_{m,i} + \frac{\mu_{m,i}^2}{\sigma_{m,i}^2} + 1} \Gamma \left(\frac{\mu_{m,i}^2}{\sigma_{m,i}^2} + 1 \right) \right]^{-1}, \quad (11)$$

where Γ is the gamma function. This likelihood function, introduced in Ref. [131], takes into account the statistical fluctuations of the MC-based predictions and of the observed data, preventing biased results and providing improved parameter coverage.

D. TGM likelihood

As mentioned earlier (Section III B 3), using TGM events together with HESE events tightens the measurement of the muon-flavor content. However, unlike HESE, there is no publicly available present-day sample of the TGM detected by IceCube [127] that we can use to compute a likelihood to the same level of detail as we do for HESE. Therefore, we do not include TGM in our present-day results, but we do when making projections of future experimental sensitivity, similarly to Refs. [51, 128].

We compute the expected number of TGM events in the i -th bin of reconstructed muon energy, $\mu_{\text{TGM},i}$, by convolving the fluxes of atmospheric plus astrophysical neutrinos, the latter of which depends on the model pa-

rameters, Θ_{\oplus} or Θ_S , with the effective detector area for the detection of TGM, and add the subdominant contribution of atmospheric muons. TGM events are dominated by atmospheric neutrinos, especially at LE; we fix their flux to the computation by MCEq with cosmic-ray flux model H3a, hadronic model SIBYLL-2.3c and atmosphere model NRLMSISE-00 [132–135].

We compute TGM event rates using the PLE ν M framework [129], which estimates the effective area of future neutrino telescopes as a function of declination by rotating the IceCube effective area to the detector position and scaling it by the detector size. The IceCube effective area is based on a recent public IceCube point-source data release [136]. The computation of event rates includes the same energy smearing provided in the data release, to account for event reconstruction effects. Because of the difficulty in modeling the contamination of atmospheric muons in the sample, which dominate for down-going events, we only consider up-going events, where the contamination is small. The event selection of the IceCube point-source sample is different from the TGM event selection used for diffuse flux measurements

in, *e.g.*, Ref. [127], and contains a higher atmospheric background. However, since we do not use the point-source data directly in our work, but only its associated detector effective area determined by simulation for an up-going neutrino flux, we do not expect a notable difference between basing our results on it *vs.* basing them on the alternative TGM event selection that is used for diffuse flux measurements.

The way we generate our samples of TGM results in them including also HESE tracks, *i.e.*, tracks that start inside the detector volume, which can lead to overcounting when combined with HESE data. However, this is not significant, since the number of HESE tracks is far smaller than the number of TGM; see Section III B 2.

We include the contribution of TGM via the Poisson likelihood

$$\mathcal{L}_{\text{TGM}}(\Theta) = e^{-\mu_{\text{TGM}}(\Theta)} \prod_i^{\text{bins}} \frac{(N_{\text{TGM},i})^{-\mu_{\text{TGM},i}(\Theta)}}{N_{\text{TGM},i}!}, \quad (12)$$

where the product is over bins of reconstructed muon energy, E_μ , each of size 0.2 in $\log_{10}(E_\mu/\text{GeV})$, $\mu_{\text{TGM}} \equiv \sum_i \mu_{\text{TGM},i}$ is the total number of events across all bins, and $N_{\text{TGM},i}$ is the number of observed tracks in the projected mock event sample. Unlike the HESE sample, where the events have a rather high energy threshold of 60 TeV, we count TGM with energies $E_\mu \gtrsim 100$ GeV.

E. Combined HESE and TGM likelihood

In our projections, for a choice of astrophysical neutrino spectrum shape and flavor composition from among our benchmarks, we generate mock samples of HESE events, $N_{c,i}$, $N_{\text{tr},i}$, $N_{\text{dc},i}$, and of TGM events, $N_{\text{TGM},i}$. With them, we compute the combined likelihood

$$\mathcal{L}(\Theta) = \mathcal{L}_{\text{TGM}}(\Theta)\mathcal{L}_{\text{HESE}}(\Theta). \quad (13)$$

F. Posterior and parameter optimization

Based on the above likelihood functions, we compute the joint parameter posterior,

$$\mathcal{P}(\Theta) = \mathcal{L}(\Theta)\pi(\Theta), \quad (14)$$

where $\pi(\Theta)$ is the joint prior distribution of the model parameters. Table II shows our choices of priors. We maximize the posterior numerically, using Markov Chain Monte Carlo methods implemented in UltraNest [137–139], an efficient Bayesian importance sampler. Later, we report two-dimensional credible intervals of the flavor content by marginalizing over all other parameters (Fig. 3). In Appendix A, we also report one-dimensional intervals for selected parameters.

V. RESULTS

First (Section V A), we show measurements of the LE and HE flavor composition at Earth, for each of our benchmark scenarios of neutrino spectrum, using present-day IceCube HESE events and projected event samples detected by future neutrino telescopes. Then (Section V B), we quantify the power to infer the presence of a flavor transition via Bayes factors that contrast the evidence for descriptions of the observed data with and without a flavor transition. Finally (Section V C), we infer the flavor composition at the sources for each of our benchmark scenarios.

A. Flavor composition at Earth

We compute the posterior distributions corresponding to the flavor composition at Earth using the methods outlined in Section IV, separately for each of our three benchmark neutrino spectra: PL, BPL, and Step. For our present-day results, we use the IceCube 7.5-year HESE sample [16, 17]. For our projections, we assume that the true flavor composition is that of pion decay below the transition energy, E_{trans} , and muon-damped above it; we show results assuming $E_{\text{trans}} = 200$ TeV and 1 PeV. We extract the flavor composition at LE (below E_{trans}) and HE (above E_{trans}) using the methods presented in Section IV.

Figure 3 shows the resulting posterior distributions of the flavor composition. At present, due to the limited size of the HESE sample, the 68% credible regions cover nearly the entire flavor triangle regardless of the choice of benchmark spectrum. The measured transition energy assuming the PL flux is $E_{\text{trans}} \approx 193_{-87}^{+2777}$ TeV. The large errors render the measurement meaningless; we find similar results the BPL and Step fluxes (see Table A1 in Appendix A). The large errors reflect the fact that there is no statistically significant evidence for a flavor transition in present-day HESE data; we quantify later (Section V B). Appendix A shows the joint posteriors and one-dimensional marginalized allowed ranges of the free model parameters, including the flavor composition.

Figure 3 also shows important improvement in the projected measurements in the milestone years 2040, 2050, and 2060, though results for the latter two milestones should be taken to be especially tentative. The improvement in between today and 2040 is vast: the uncertainty at the 68% C.L. shrinks by a factor of 5–6 for both LE and HE. After 2040, the improvement slows down because the fractional increase in the combined detector exposure over time is smaller and because the measurement becomes increasingly marred by systematic uncertainties such as the event reconstruction capabilities of the detectors, whose improvement over time, while likely, is not factored into our projections.

Figure 4 illustrates one of the two factors behind the improvement in the projected measurements: includ-

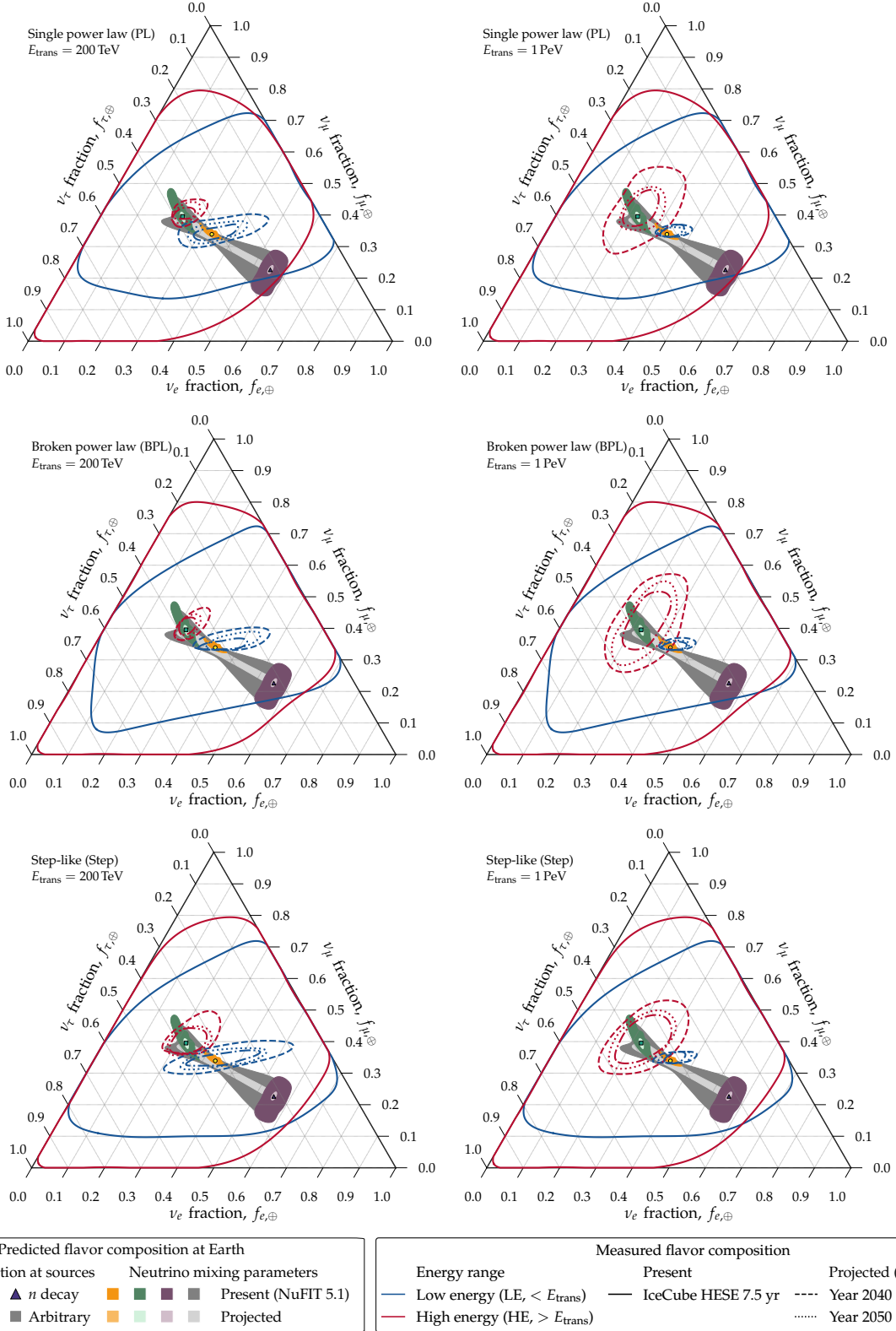


FIG. 3. *Flavor composition of high-energy astrophysical neutrinos measured at Earth, at LE and HE.* Present measurements are from the IceCube 7.5-year HESE sample [16, 17]; projected measurements, from the detection of HESE plus TGM by multiple neutrino telescopes (Table I). Results are for three benchmark neutrino spectra (Fig. 2)—PL (top), BPL (center), and Step (bottom)—that transition at $E_{\text{trans}} = 200$ TeV (left) or 1 PeV (right). For projections, the transition is from pion decay at LE to muon-damped at HE. The predicted regions of flavor composition at Earth are from standard oscillations [19, 36] Table II). All regions are at 68% C.L. See Section V A for details. *There is no evidence of a flavor transition with energy in present HESE data, but projections reveal sensitivity to detect one.*

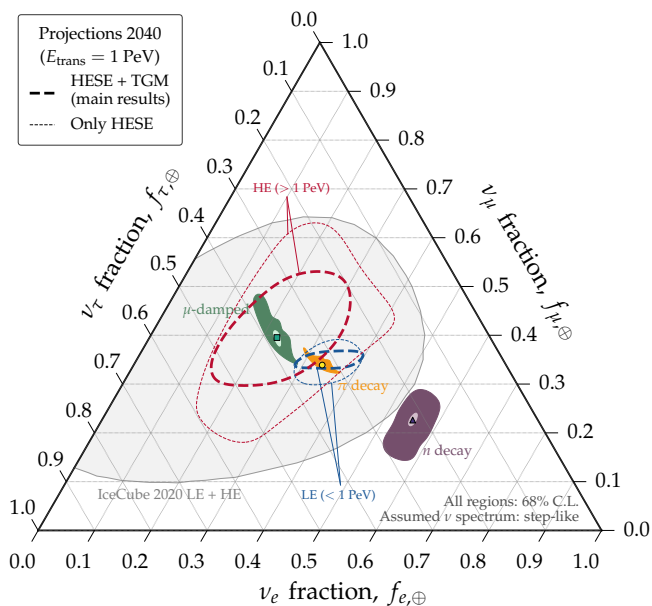


FIG. 4. *Improvement in flavor-composition measurements due to TGM.* This plot shows projections for the year 2040. Our main results are generated using HESE plus TGM; for comparison, we show results generated using only HESE. The neutrino spectrum is assumed to be step-like (Fig. 2). Previous energy-averaged measurements are from IceCube (“IceCube 2020 LE + HE”) [18]. The allowed flavor regions for neutrino production via pion decay, muon-damped production, and neutron decay are computed as in Ref. [19], assuming present-day [20, 21] and projected [19] uncertainties in the neutrino mixing parameters. See Section V A and Fig. A3 in Appendix A for details. *Using TGM improves the measurement of the ν_μ content roughly by a factor of 2.*

ing though-going muons shrinks the measurement errors mainly in the $f_{\mu,\oplus}$ direction. The second factor is the large increase in the combined exposure of upcoming detectors (Fig. 5) to HESE events, which shrinks the measurement errors mainly in the $f_{e,\oplus}$ direction, as evidenced by comparing Figs. 4 and 3.

The key to achieving the sensitivity to a flavor transition is the value of the transition energy, which determines the number of events from which to measure the flavor composition in the LE and HE regions. If the flavor transition were to happen at too low or too high an energy, the number of events in the LE or HE region would not be large enough to pin down the flavor composition in that region, thus curbing attempts to identify the transition. Therefore, neutrino telescopes are most sensitive to an intermediate transition energy.

Nevertheless, Fig. 3 shows that future measurements should be able to distinguish between the LE and HE flavor composition, for both of our choices E_{trans} , 200 TeV and 1 PeV, and regardless of the flux model used. The sizes of the 68% C.L. allowed regions of flavor composition are comparable for all flux models. By 2040, the distinction is marginal at 68% C.L.; by 2050, it reaches

95% C.L. (not shown). Given that the neutrino flux falls steeply with energy, a value of E_{trans} of 200 TeV splits the event samples more evenly between LE and HE than a value of 1 PeV. As a result, Fig. 3 shows that, for $E_{\text{trans}} = 200$ TeV, the measurements at LE and HE have comparable uncertainty, with HE marginally worse than LE, while for $E_{\text{trans}} = 1$ PeV the measurement at HE is about a factor-of-3 more uncertain than at LE, due to the paucity of events in the HE region.

Although the measurement uncertainty of the flavor composition is comparable for the PL, BPL, and Step flux models, the precision with which E_{trans} is measured is different in each of them. For instance, assuming 200 TeV as the true value of E_{trans} , its best-fit measured value is measured accurately between 191–199 TeV, depending on the flux model, but the 68% C.L. precision is about 53% for PL, 9% for BPL, and 5% for Step. The precision obtained when assuming a true value of 1 PeV is similar; Table A1 shows the full results.

This hierarchy in precision among flux models is unsurprising: in the PL model, any evidence of flavor transition stems solely from the change in the flavor composition, while in the BPL and Step models, it comes also, and dominantly, from the change in the shape of the spectrum at E_{trans} (Fig. 2). The precision is highest for the Step model because the change in the spectrum is the largest among our benchmark models; this is most evident when the transition is at 1 PeV (Table A2). It is auspicious that the Step model is closest to what a realistic flavor transition from pion decay to muon-damped might look like.

B. Quantifying the evidence for a flavor transition

Next, we quantify the preference for the presence of a flavor transition via a Bayes factor that compares the Bayesian evidence for a scenario explaining the observed events that posits a transition *vs.* a scenario that does not. The evidence is the integral of the posterior, \mathcal{P} in Eq. (14), over the entire space of model parameter, Θ , *i.e.*, $\mathcal{Z} = \int d\Theta \mathcal{P}(\Theta)$. The Bayes factor comparing two scenarios, A and B, respectively with evidence \mathcal{Z}_A and \mathcal{Z}_B , is $\mathcal{B} \equiv \mathcal{Z}_A/\mathcal{Z}_B$. The higher the value of \mathcal{B} , the stronger the evidence in favor of scenario A over B is in the observations. We adopt Jeffreys’ criteria [140] to interpret the values of the Bayes factor (Fig. 5): $0 \leq \log_{10} \mathcal{B} < 0.5$ represents evidence for scenario A that is barely worth mentioning; $0.5 \leq \log_{10} \mathcal{B} < 1$, substantial evidence; $1 \leq \log_{10} \mathcal{B} < 1.5$, strong evidence; $1.5 \leq \log_{10} \mathcal{B} < 2$, very strong evidence; and $\log_{10} \mathcal{B} \geq 2$, decisive evidence.

Table III shows the two sets of Bayes factors that we compute: \mathcal{B}_1 and \mathcal{B}_2 . Via \mathcal{B}_1 , we assess the preference for a scenario with a flavor and spectrum transition—scenario A, computed in turn for PL, BPL, and Step—*vs.* a scenario with no flavor or spectrum transition—scenario B, fixed to PL with $f_{\alpha,\oplus}^{\text{LE}} = f_{\alpha,\oplus}^{\text{HE}}$. Via \mathcal{B}_2 , we

TABLE III. *Scenarios of model comparison, quantified via Bayes factors.* We explore two scenarios: one where evidence for a transition from LE to HE in the diffuse neutrino flux stems from flavor and spectrum changes, \mathcal{B}_1 , and another where it stems from flavor changes only, \mathcal{B}_2 . In all cases, the evidence \mathcal{Z}_B is evaluated assuming no flavor transition, *i.e.*, $f_{\alpha,\oplus}^{\text{LE}} = f_{\alpha,\oplus}^{\text{HE}}$ ($\alpha = e, \mu, \tau$). We compute Bayes factors for our benchmark neutrino spectra (Section II A)—single power law (PL), broken power law (BPL), and step-like (Step). See Fig. 5 for results based on present and projected data, and Section V B for details.

Bayes factor, $\mathcal{Z}_A/\mathcal{Z}_B$	What it tests	Statistical evidence computed with	
		\mathcal{Z}_A	\mathcal{Z}_B
\mathcal{B}_1	Flavor and spectrum transition <i>vs.</i> no flavor nor spectrum transition	PL	PL with $f_{\alpha,\oplus}^{\text{LE}} = f_{\alpha,\oplus}^{\text{HE}}$
		BPL	PL with $f_{\alpha,\oplus}^{\text{LE}} = f_{\alpha,\oplus}^{\text{HE}}$
		Step	PL with $f_{\alpha,\oplus}^{\text{LE}} = f_{\alpha,\oplus}^{\text{HE}}$
\mathcal{B}_2	Flavor and spectrum transition <i>vs.</i> no flavor transition	PL	PL with $f_{\alpha,\oplus}^{\text{LE}} = f_{\alpha,\oplus}^{\text{HE}}$
		BPL	BPL with $f_{\alpha,\oplus}^{\text{LE}} = f_{\alpha,\oplus}^{\text{HE}}$
		Step	Step with $f_{\alpha,\oplus}^{\text{LE}} = f_{\alpha,\oplus}^{\text{HE}}$

assess the preference for a scenario with a flavor and spectrum transition—scenario A, computed in turn for PL, BPL, and Step—*vs.* a scenario with no flavor transition, only spectrum transition—scenario B, matching the same choice as for scenario A but with $f_{\alpha,\oplus}^{\text{LE}} = f_{\alpha,\oplus}^{\text{HE}}$. Thus, \mathcal{B}_1 quantifies the evidence for one of our three benchmark scenarios with flavor transition against the null hypothesis of no flavor transition and a simple power-law spectrum, whilst \mathcal{B}_2 asks the more difficult question of establishing the existence of a flavor transition without relying on an associated change in the spectrum shape.

Our present-day results are based on the IceCube 7.5-year HESE sample, and \mathcal{Z}_A and \mathcal{Z}_B are computed from it. Our projections are based on the combined detection of HESE and TGM by multiple upcoming neutrino telescopes. In the projections, we assume that the true PL, BPL, and Step fluxes are given by the parameters in Table II. These are the fluxes with which we generate the mock event samples that we assume to be the observed ones, and \mathcal{Z}_A and \mathcal{Z}_B are computed from them. We compute projections for the year 2040 and beyond; like before, after 2040 our projections should be understood to be especially tentative. We use UltraNest [137, 138] to compute the evidence by varying all free model parameters simultaneously (Section IV A).

Figure 5 shows our results. Present-day results show no preference for a flavor transition, with or without an accompanying spectrum transition, and so $\mathcal{B}_1 \approx 1$ and $\mathcal{B}_2 \approx 1$ for all flux models. The main limitation is the paucity of present data, which does not allow us to draw preference for any scenario. This aligns with our present inability to measure the flavor composition at Earth (Section V A) and at the sources (later, in Section V C).

Fortunately, our projections in Fig. 5 show that the above limitation might be overcome before 2040, possibly a decade earlier, depending on the neutrino flux. Below, we describe the features of our projections.

At any one time, \mathcal{B}_1 is larger than \mathcal{B}_2 , which reflects the fact that it is easier to find preference for a transition in energy when evidence for it comes both from a change

in flavor and in spectrum *vs.* when the spectrum is known and evidence comes only from a flavor change.

The choice of transition energy has a large effect on how soon we can obtain strong evidence for a flavor transition. We show results assuming $E_{\text{trans}} = 200$ TeV and 1 PeV. As when measuring the flavor composition at Earth (Section V A), a lower value of E_{trans} splits the number of detected neutrinos more evenly between the low- and high-energy regions, and makes it easier to spot a transition between them. As a result, Fig. 5 shows that the Bayes factor for $E_{\text{trans}} = 200$ TeV is consistently higher than for 1 PeV.

The preference for a transition in energy, quantified via \mathcal{B}_1 , is higher for the BPL and Step flux models, which have a spectrum transition associated to the flavor transition, than for the PL flux model, which does not. For the BPL and Step flux models, decisive evidence for a transition may become available already by 2030, regardless of the value E_{trans} , using only a subset of the future telescopes under consideration—IceCube, Baikal-GVD, and KM3NeT (Table I). For the PL flux model, substantial evidence may become available by 2040 if $E_{\text{trans}} = 200$ TeV, and decisive evidence would have to wait one or two more decades.

Finally, Fig. 5 shows a subtle feature in the time evolution of our projections: the Bayes factor drops at early times and grows at later times. This is because at early times \mathcal{Z}_A decreases as a result, first, of splitting up the limited number of detected events between the LE and HE regions and, second, of the fact that \mathcal{Z}_A depends on more free parameters than \mathcal{Z}_B , for which $f_{\alpha,\oplus}^{\text{LE}} = f_{\alpha,\oplus}^{\text{HE}}$ by construction. At later times, the Bayes factor instead grows, since there are enough events in the LE and HE regions for the transition between them to be identified.

Figure 6 illustrates the measurement of the energy-averaged flavor composition in a situation when in reality it features a transition in energy. In Fig. 6, the true flux is taken to be a Step spectrum with a transition at 1 PeV. Our main results, duplicated in Fig. 6 from Fig. 3, fit the observed event sample assuming also a Step spec-

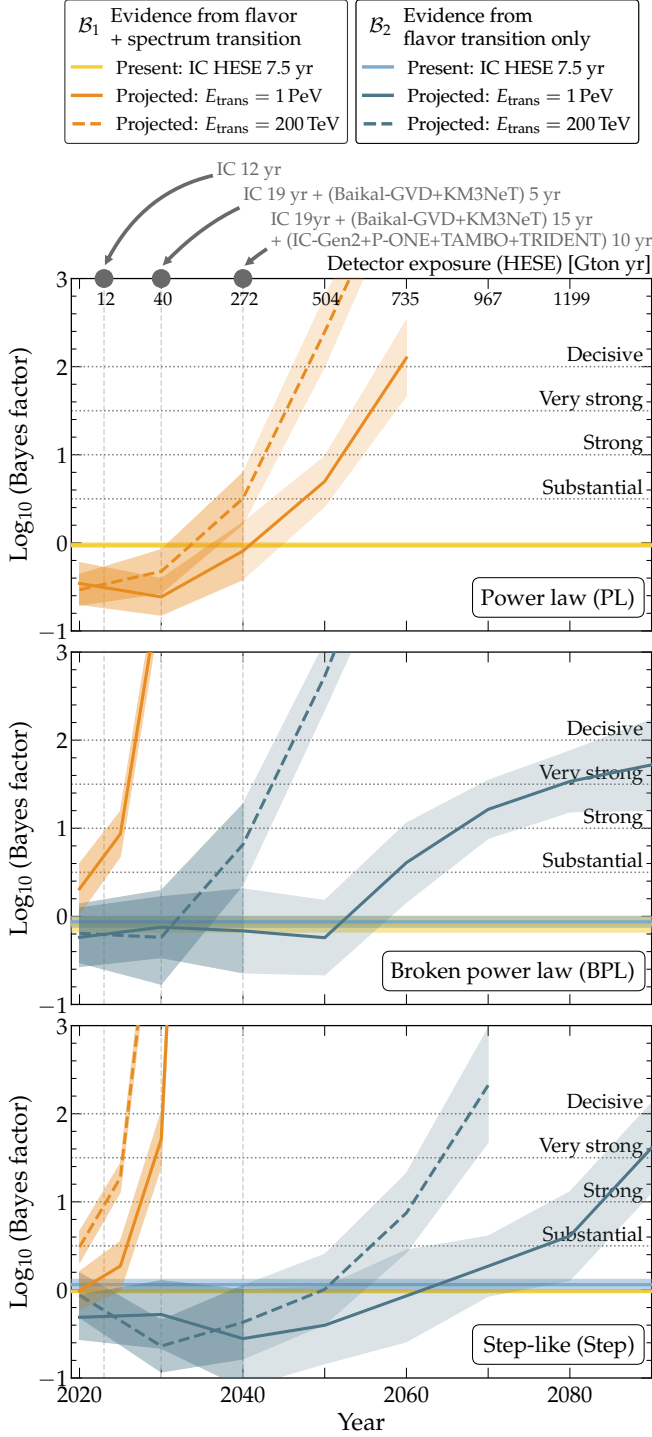


FIG. 5. *Evidence for a transition with energy in the flavor composition of high-energy astrophysical neutrinos.* Results show preferred and 68% C.L. allowed values of Bayes factors \mathcal{B}_1 and \mathcal{B}_2 (Table III). Present results are from the IceCube 7.5-year HESE sample [16, 17]; projected results, from HESE plus TGM detected by multiple neutrino telescopes (Table I). Results are for three benchmark neutrino spectra (Fig. 2)—PL (top), BPL (center), and Step (bottom)—that transition at E_{trans} . Beyond 2040, projections are especially tentative. See Section VB for details. *There is no evidence of a flavor transition in present HESE data, but it may be decisive by 2030.*

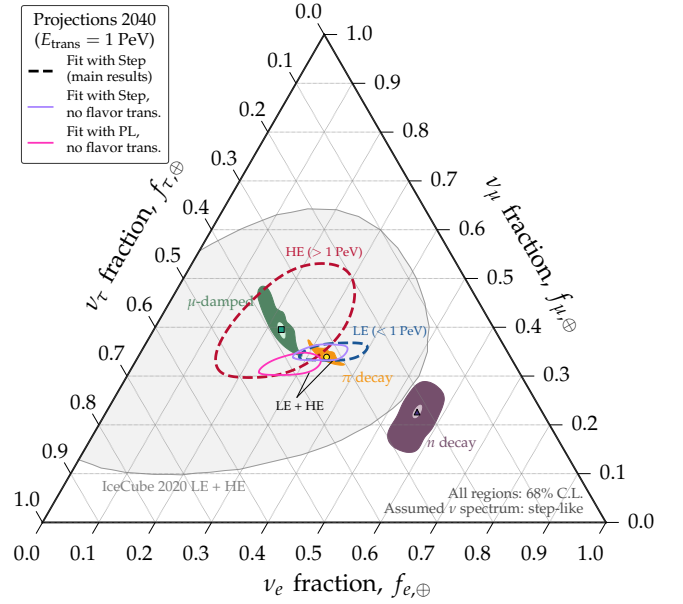


FIG. 6. *Measuring the energy-averaged flavor composition when it contains a flavor transition in energy.* For this figure, projections are for the year 2040. The neutrino spectrum is assumed to be step-like (Step), with a transition at 1 PeV (Fig. 2). Our main results report the LE and HE flavor composition separately. We contrast them against measurements of the energy-averaged flavor composition assuming step-like and single-power-law (PL) flux models without a flavor transition. Previous energy-averaged measurements from IceCube and allowed flavor regions are the same as in Fig. 4. See Section VB for details. *Flavor measurements must use flexible descriptions of the neutrino spectrum to avoid reporting inaccurate flavor-composition measurements.*

trum, and measure the LE and HE flavor composition separately. Figure 6 shows that the measurement of the energy-averaged flavor composition using the same event sample is affected by using a description of the neutrino flux that is unable to reproduce the true flux.

First, fitting the observations using a Step spectrum but without allowing a flavor composition, *i.e.*, fixing $f_{\alpha,\oplus}^{\text{LE}} = f_{\alpha,\oplus}^{\text{HE}}$, improves the measurement precision of the energy-averaged flavor composition compared to our main results for LE and HE, but erases the evidence for the muon-damped flavor composition at high energy. More extremely, fitting the observations with a PL spectrum without allowing a flavor composition yields a preferred energy-averaged flavor composition that matches neither the pion-decay nor the muon-damped benchmarks. Thus, Fig. 6 points out the need to use a flexible description of the neutrino spectrum when measuring the flavor composition, even the energy-averaged one.

C. Flavor composition at the sources

Finally, we turn to the reconstruction of the flavor composition at the sources, using the method from Ref. [52] (see also Ref. [19]). As stated in Section IV B, we assume there is no ν_τ production in the sources, and so we infer only the LE and HE fractions of ν_e at the sources, $f_{e,S}^{\text{LE}}$ and $f_{e,S}^{\text{HE}}$, which completely determine the flavor composition at the sources, *i.e.*, $(f_{e,S}^{\text{LE}}, f_{\mu,S}^{\text{LE}} \equiv 1 - f_{e,S}^{\text{LE}}, f_{\tau,S}^{\text{LE}} \equiv 0)$, and similarly for HE.

Figure 7 shows the resulting posteriors of $f_{e,S}^{\text{LE}}$ and $f_{e,S}^{\text{HE}}$. Table A2 in Appendix A shows the allowed intervals. Our present-day results, generated assuming the 7.5-year IceCube HESE sample and the NuFIT 5.1 [20, 21] distributions of the neutrino mixing parameters (Table II) are rather flat posteriors for LE and HE for all three benchmark flux models. Therefore, presently, there is no strong preference for any specific flavor composition at LE or HE at the sources, nor for the existence of a flavor transition.

This contrasts with the results of Refs. [19, 52], which reported mild preference for the energy-averaged flavor composition at the sources being muon-damped, and a clear rejection of the composition from neutron decay. In our analysis, similar conclusions cannot be reached at present for LE and HE separately, due primarily to splitting the limited number of HESE events among them.

Figure 7 also shows projections for the year 2040, generated assuming the combined detection of HESE and TGM by multiple detectors (Table I) and forecasts of higher-precision knowledge of the mixing parameters (Table II). The widths of the posterior distributions are sensitive to the value of E_{trans} , which determines the number of events in the LE and HE regions, similarly to Section V A. We show results assuming a true value of E_{trans} of 200 TeV and 1 PeV.

In our projections, the flavor composition is measured accurately, with best-fit values of $f_{e,S}^{\text{LE}} \approx 0.34$ and $f_{e,S}^{\text{HE}} \approx 0$, matching the true values of our pion-decay and muon-damped benchmarks (Fig. 2), and a 68% C.L. precision of 6–12%, depending on the flux model. Figure 7 shows that this level of precision is sufficient to distinguish between the flavor composition at LE and HE, and to firmly disfavor the flavor composition coming from neutron decay, *i.e.*, $(1 : 0 : 0)_S$, in both energy regions.

Like for the flavor composition at Earth (Table A1), the measurement uncertainty of the flavor composition at the sources is comparable for the PL, BPL, and Step flux models, but the precision on E_{trans} is different in each of them, though better overall. At 68% C.L., it is 12% for PL, 2% for BPL, and 2% for Step (Table A2). Compared to the measurement of the flavor composition at the Earth, the precision of the inferred flavor composition at the sources is better as a result of having to fit a single flavor fraction at LE and HE, rather than two.

VI. ENVISIONED IMPROVEMENTS

Our methods and results are sound and informed by realistic detector capabilities, but we envision opportunities for improvement. Below, we list three salient ones.

Refined treatment of future detectors: Our analysis above relies on current IceCube event-reconstruction capabilities, and assume that future detectors will have different sizes but detection capabilities comparable to IceCube. However, in reality, the capabilities of a future detector depend on its components, layout, and detection medium, which we do not account for. For example, in IceCube-Gen2, a 250-m spacing between detector strings would make HESE detection efficient above 200 TeV, rather than above 60 TeV as in IceCube, which has a 125-m spacing [54]. Further, the timeline we have adopted for upcoming detectors is tentative and subject to change, and may be augmented by even larger detectors, like the recently proposed HUNT [110]. It may unfurl at a different—and, we hope, faster—rate. Our projections may be refined as updated information becomes publicly available on the design, capabilities, and timeline of future detectors.

Using lower-energy events: In our analysis, we have used HESE and TGM events, which have energies larger than 60 TeV and 100 GeV, respectively. Including events with lower energies would not only increase the combined size of the event sample, but extend the energy range of the analysis down to 1 TeV. For instance, preliminary studies show that using IceCube Medium-Energy Starting Events (MESE) would yield more precise flavor measurements than HESE at LE [141]. However, since there is presently no MC event sample of lower-energy events publicly available, we do not include them in our analysis for now.

Progress in event reconstruction: Measurements of the flavor composition may be improved by ongoing progress in event reconstruction [142–144] and advances in flavor identification based on using dedicated templates [18, 145] and muon and neutron echoes [146–148].

VII. SUMMARY AND OUTLOOK

The flavor composition of TeV–PeV astrophysical neutrinos, *i.e.*, the relative proportion of ν_e , ν_μ , and ν_τ in their flux, plays an important role in revealing the neutrino production mechanisms, the features and identities of their largely unknown astrophysical sources, and potential new physics. Due to the difficulty in identifying flavor in high-energy neutrino telescopes and to a limited number of detected neutrinos, previous studies have

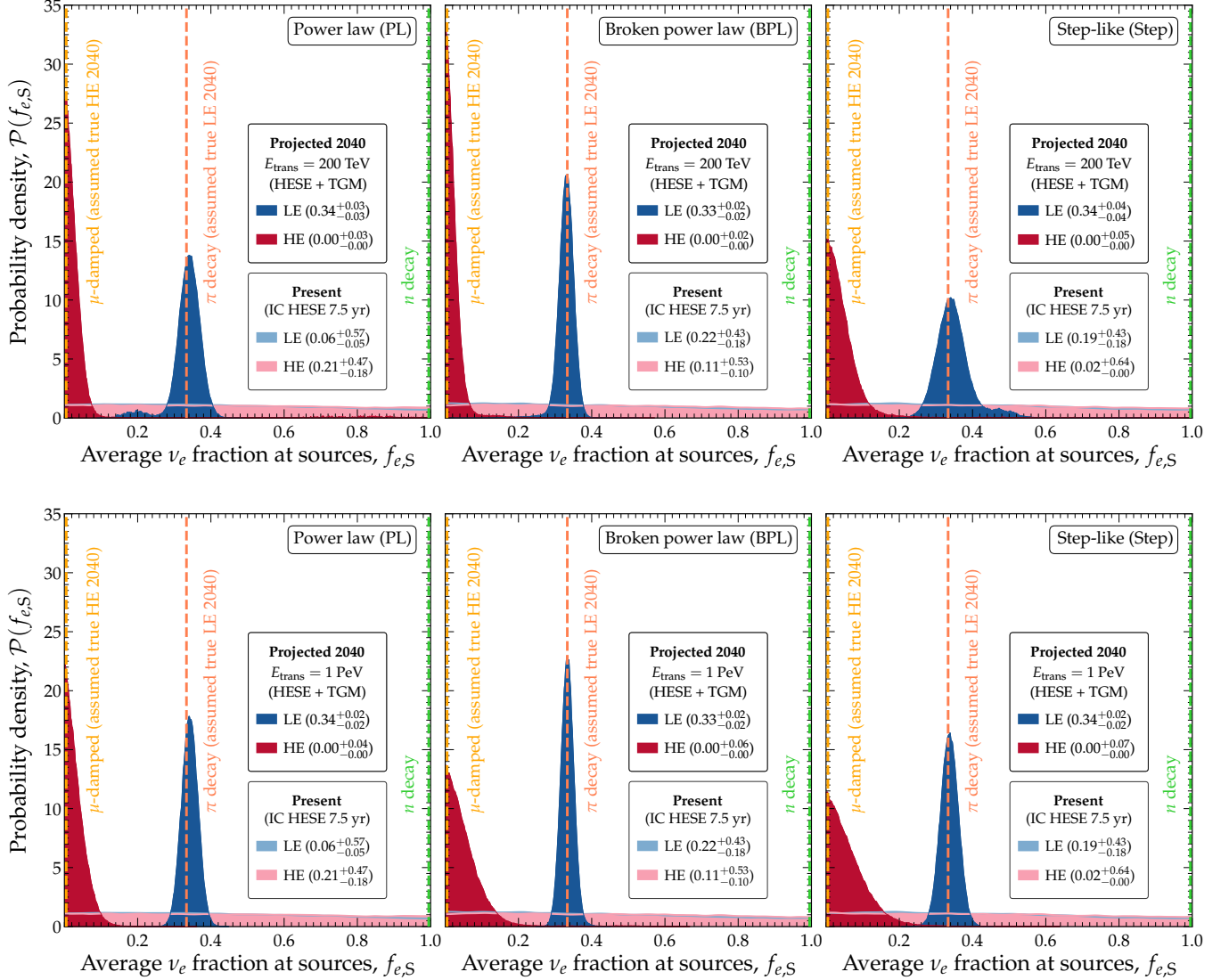


FIG. 7. *Inferred posterior distribution of the fraction of high-energy astrophysical neutrinos produced as ν_e , at LE and HE.* Present results are from the IceCube 7.5-year HESE sample [16, 17], using the presently allowed values of the neutrino mixing parameters from NuFIT 5.1 [20, 21]. Projected results are for the year 2040 and use the combined, cumulative detection of HESE and TGM events by multiple neutrino telescopes (Table I), and projected measurements of the mixing parameters (Table II). The projections are made for three benchmark neutrino spectra (Fig. 2)—PL (left), BPL (center), and Step (right)—which transition from pion decay at LE to muon-damped at HE, *i.e.*, below and above E_{trans} . We show results for $E_{\text{trans}} = 200$ TeV (top) and 1 PeV (bottom). The allowed intervals of flavor composition are at 68% C.L. See Table A2 for further results and Section VC for details. *There is no evidence of a flavor transition with energy in present HESE data, but projections reveal sensitivity to differentiate between the pion-decay, muon-damped, and neutron-decay neutrino production mechanisms at LE and HE.*

measured the flavor composition at Earth under the assumption that it is constant over the observed range of neutrino energies, or averaging it over this range.

Yet, in actuality, the flavor composition likely varies with neutrino energy, as different physical processes driving neutrino production, with different yields of ν_e , ν_μ , and ν_τ , act at different energies, or as new-physics effects become relevant at different energies. When measuring the energy-averaged flavor composition, the above effects were washed out and are harder to spot, eroding the in-

sight on them that we can hope to extract.

To remedy this, we have reported the first measurements of the energy dependence of the high-energy neutrino flavor composition. Our methods build on the experience of previous flavor measurements, and rely on nuanced modeling of the detection capabilities of IceCube to provide robust results based on present-day data and informed projections for the next two decades. Today, the measurement is challenging, due to the limited number of detected events. In the near future, the growing

number of events detected by upcoming neutrino telescopes is bound to increase the precision substantially.

We have assessed the capability to measure a transition in the flavor composition from low to high neutrino energy. Rather than studying specific models of neutrino production or new physics, we have explored three benchmark models of the neutrino energy spectrum that represent the breadth of predictions: a single unbroken power law (PL), a broken power law (BPL), and a step-like spectrum (Step) with a large change in flux normalization. Each model includes a transition in the flavor composition from low to high energy. In our projections, we assume the flavor composition at LE to be given by the full pion decay chain, $(1 : 2 : 0)_S$, and, at high energies, by muon-damped pion decay, $(0 : 1 : 0)_S$. In the BPL and Step models, the flavor transition happens concomitantly with a break in the power-law spectrum or a change in its normalization, respectively.

For our present-day results, we use the publicly available IceCube 7.5-year sample of High-Energy Starting Events (HESE). Because of the paucity of events in the sample, we are unable to identify the presence of a flavor transition. Unsurprisingly, the error in the flavor composition measured at low and high energy covers nearly the full space of possibilities, even at 68% C.L.

For our projections, we use the detection of HESE events plus through-going muons (TGM) by IceCube and by future neutrino telescopes Baikal-GVD, IceCube-Gen2, KM3NeT, P-ONE, TAMBO, and TRIDENT. Using multiple telescopes, most of which are larger than IceCube, boosts the detection rate of HESE. Adding TGM events improves the measurement of the ν_μ content.

By the year 2040, it might be possible to identify a flavor transition at an energy of 1 PeV and, marginally, to distinguish between the flavor composition at low and high energies, thanks to a reduction in the uncertainty of its measurement in a factor of 5–6. The distinction is marginal due to the rarity of events above 1 PeV. The significance of these claims improves if the transition occurs instead at 200 TeV, which entails a more even splitting of events between low and high energies. However, identifying a transition in the flavor composition without relying on identifying also an associated change in the spectrum shape might require observations beyond 2040.

The above measurements of the flavor composition at Earth, combined with projected high-precision knowl-

edge of the neutrino mixing parameters, would allow us to infer the flavor composition with which neutrinos are produced at their sources. By 2040, we could measure the low- and high-energy flavor composition accurately, with a precision of 6–12%. This is enough to establish the full pion decay as the main neutrino production mechanism at LE and muon-damped production at HE, and to discard alternatives like production via neutron decay.

Overall, our findings show that the measurement of the flavor composition at different energies is challenging today, but is set to improve appreciably in the near future. Pursuing it will strengthen and broaden the insight into neutrino astrophysics and fundamental physics that flavor measurements deliver.

ACKNOWLEDGMENTS

The authors would like to thank Paschal Coyle, Francis Halzen, Elisa Resconi, and Véronique van Elewycq, and Donglian Xu for helpful discussion. The authors also thank Fan Hu for providing TRIDENT effective areas. CAA is supported by the Faculty of Arts and Sciences of Harvard University and was partially supported by the Alfred P. Sloan Foundation in this work, and by the NSF CAREER Award PHY-2239795. MB and DFGF are supported by the Villum Fonden under Project No. 29388. This project has received funding from the European Union’s Horizon 2020 research and innovation program under the Marie Skłodowska-Curie Grant Agreement No. 847523 ‘INTERACTIONS’. QL and ACV are supported by the Arthur B. McDonald Canadian Astroparticle Physics Research Institute, with equipment funded by the Canada Foundation for Innovation and the Province of Ontario, and housed at the Queen’s Centre for Advanced Computing. Research at Perimeter Institute is supported by the Government of Canada through the Department of Innovation, Science, and Economic Development, and by the Province of Ontario. ACV acknowledges further support from NSERC and the Ontario Ministry of Colleges and Universities. NS is supported by the National Natural Science Foundation of China (NSFC) Project No. 12047503. NS also acknowledges the UK Science and Technology Facilities Council for support through the Quantum Sensors for the Hidden Sector collaboration under the grant ST/T006145/1.

* qinrui.liu@queensu.ca

† damiano.fiorillo@nbi.ku.dk

‡ carguelles@fas.harvard.edu

§ mbustamante@nbi.ku.dk

¶ songnq@itp.ac.cn

** aaron.vincent@queensu.ca

[1] W. Pauli, Dear radioactive ladies and gentlemen, *Phys. Today* **31N9**, 27 (1978).

[2] L. A. Anchordoqui *et al.*, Cosmic Neutrino Pevatrons: A Brand New Pathway to Astronomy, Astrophysics, and Particle Physics, *JHEAp* **1-2**, 1 (2014), arXiv:1312.6587 [astro-ph.HE].

[3] M. Ahlers and F. Halzen, Opening a New Window onto the Universe with IceCube, *Prog. Part. Nucl. Phys.* **102**, 73 (2018), arXiv:1805.11112 [astro-ph.HE].

[4] M. Ackermann *et al.*, Astrophysics Uniquely Enabled by Observations of High-Energy Cosmic Neutrinos, *Bull.*

- Am. Astron. Soc. **51**, 185 (2019), [arXiv:1903.04334](https://arxiv.org/abs/1903.04334) [[astro-ph.HE](#)].
- [5] P. Mészáros, D. B. Fox, C. Hanna, and K. Murase, Multi-Messenger Astrophysics, *Nature Rev. Phys.* **1**, 585 (2019), [arXiv:1906.10212](https://arxiv.org/abs/1906.10212) [[astro-ph.HE](#)].
- [6] F. Halzen and A. Kheirandish, Multimessenger Search for the Sources of Cosmic Rays Using Cosmic Neutrinos, *Front. Astron. Space Sci.* **6**, 32 (2019).
- [7] A. Palladino, M. Spurio, and F. Vissani, Neutrino Telescopes and High-Energy Cosmic Neutrinos, *Universe* **6**, 30 (2020), [arXiv:2009.01919](https://arxiv.org/abs/2009.01919) [[astro-ph.HE](#)].
- [8] R. Alves Batista *et al.*, EuCAPT White Paper: Opportunities and Challenges for Theoretical Astroparticle Physics in the Next Decade, (2021), [arXiv:2110.10074](https://arxiv.org/abs/2110.10074) [[astro-ph.HE](#)].
- [9] M. Ackermann *et al.*, High-energy and ultra-high-energy neutrinos: A Snowmass white paper, *JHEAp* **36**, 55 (2022), [arXiv:2203.08096](https://arxiv.org/abs/2203.08096) [[hep-ph](#)].
- [10] C. Guépin, K. Kotera, and F. Oikonomou, High-energy neutrino transients and the future of multimessenger astronomy, *Nature Rev. Phys.* **4**, 697 (2022), [arXiv:2207.12205](https://arxiv.org/abs/2207.12205) [[astro-ph.HE](#)].
- [11] T. K. Gaisser, F. Halzen, and T. Stanev, Particle astrophysics with high-energy neutrinos, *Phys. Rept.* **258**, 173 (1995), [Erratum: *Phys. Rept.* 271, 355 (1996)], [arXiv:hep-ph/9410384](https://arxiv.org/abs/hep-ph/9410384).
- [12] M. Ahlers, K. Helbing, and C. Pérez de los Heros, Probing Particle Physics with IceCube, *Eur. Phys. J. C* **78**, 924 (2018), [arXiv:1806.05696](https://arxiv.org/abs/1806.05696) [[astro-ph.HE](#)].
- [13] M. Ackermann *et al.*, Fundamental physics with high-energy cosmic neutrinos, *Bull. Am. Astron. Soc.* **51**, 215 (2019), [arXiv:1903.04333](https://arxiv.org/abs/1903.04333) [[astro-ph.HE](#)].
- [14] C. A. Argüelles, M. Bustamante, A. Kheirandish, S. Palomares-Ruiz, J. Salvadó, and A. C. Vincent, Fundamental physics with high-energy cosmic neutrinos today and in the future, *PoS ICRC2019*, 849 (2020), [arXiv:1907.08690](https://arxiv.org/abs/1907.08690) [[astro-ph.HE](#)].
- [15] C. A. Argüelles *et al.*, Snowmass white paper: beyond the Standard Model effects on neutrino flavor: Submitted to the proceedings of the US community study on the future of particle physics (Snowmass 2021), *Eur. Phys. J. C* **83**, 15 (2023), [arXiv:2203.10811](https://arxiv.org/abs/2203.10811) [[hep-ph](#)].
- [16] R. Abbasi *et al.* (IceCube), The IceCube high-energy starting event sample: Description and flux characterization with 7.5 years of data, *Phys. Rev. D* **104**, 022002 (2021), [arXiv:2011.03545](https://arxiv.org/abs/2011.03545) [[astro-ph.HE](#)].
- [17] IceCube Collaboration, HESE 7.5 year data release, <https://icecube.wisc.edu/data-releases/2021/12/hese-7-5-year-data/> (2021).
- [18] R. Abbasi *et al.* (IceCube), Detection of astrophysical tau neutrino candidates in IceCube, *Eur. Phys. J. C* **82**, 1031 (2022), [arXiv:2011.03561](https://arxiv.org/abs/2011.03561) [[hep-ex](#)].
- [19] N. Song, S. W. Li, C. A. Argüelles, M. Bustamante, and A. C. Vincent, The Future of High-Energy Astrophysical Neutrino Flavor Measurements, *JCAP* **04**, 054, [arXiv:2012.12893](https://arxiv.org/abs/2012.12893) [[hep-ph](#)].
- [20] I. Esteban, M. González-García, M. Maltoni, T. Schwetz, and A. Zhou, The fate of hints: updated global analysis of three-flavor neutrino oscillations, *JHEP* **09**, 178, [arXiv:2007.14792](https://arxiv.org/abs/2007.14792) [[hep-ph](#)].
- [21] NuFIT 5.1, <http://www.nu-fit.org/?q=node/238> (2021).
- [22] M. G. Aartsen *et al.* (IceCube), The IceCube Neutrino Observatory: Instrumentation and Online Systems, *JINST* **12** (03), P03012, [arXiv:1612.05093](https://arxiv.org/abs/1612.05093) [[astro-ph.IM](#)].
- [23] I. A. Belolaptikov *et al.* (BAIKAL), The Baikal underwater neutrino telescope: Design, performance and first results, *Astropart. Phys.* **7**, 263 (1997).
- [24] J. Ahrens *et al.* (AMANDA), Search for extraterrestrial point sources of neutrinos with AMANDA-II, *Phys. Rev. Lett.* **92**, 071102 (2004), [arXiv:astro-ph/0309585](https://arxiv.org/abs/astro-ph/0309585).
- [25] M. Ageron *et al.* (ANTARES), ANTARES: the first undersea neutrino telescope, *Nucl. Instrum. Meth. A* **656**, 11 (2011), [arXiv:1104.1607](https://arxiv.org/abs/1104.1607) [[astro-ph.IM](#)].
- [26] J. G. Learned and K. Mannheim, High-energy neutrino astrophysics, *Ann. Rev. Nucl. Part. Sci.* **50**, 679 (2000).
- [27] M. G. Aartsen *et al.* (IceCube), Evidence for High-Energy Extraterrestrial Neutrinos at the IceCube Detector, *Science* **342**, 1242856 (2013), [arXiv:1311.5238](https://arxiv.org/abs/1311.5238) [[astro-ph.HE](#)].
- [28] M. G. Aartsen *et al.* (IceCube), Observation of High-Energy Astrophysical Neutrinos in Three Years of IceCube Data, *Phys. Rev. Lett.* **113**, 101101 (2014), [arXiv:1405.5303](https://arxiv.org/abs/1405.5303) [[astro-ph.HE](#)].
- [29] M. G. Aartsen *et al.* (IceCube, Fermi-LAT, MAGIC, AGILE, ASAS-SN, HAWC, H.E.S.S., INTEGRAL, Kanata, Kiso, Kapteyn, Liverpool Telescope, Subaru, Swift NuSTAR, VERITAS, VLA/17B-403), Multimessenger observations of a flaring blazar coincident with high-energy neutrino IceCube-170922A, *Science* **361**, eaat1378 (2018), [arXiv:1807.08816](https://arxiv.org/abs/1807.08816) [[astro-ph.HE](#)].
- [30] M. G. Aartsen *et al.* (IceCube), Neutrino emission from the direction of the blazar TXS 0506+056 prior to the IceCube-170922A alert, *Science* **361**, 147 (2018), [arXiv:1807.08794](https://arxiv.org/abs/1807.08794) [[astro-ph.HE](#)].
- [31] R. Abbasi *et al.* (IceCube), Evidence for neutrino emission from the nearby active galaxy NGC 1068, *Science* **378**, 538 (2022), [arXiv:2211.09972](https://arxiv.org/abs/2211.09972) [[astro-ph.HE](#)].
- [32] J. G. Learned and S. Pakvasa, Detecting tau-neutrino oscillations at PeV energies, *Astropart. Phys.* **3**, 267 (1995), [arXiv:hep-ph/9405296](https://arxiv.org/abs/hep-ph/9405296).
- [33] S. Pakvasa, W. Rodejohann, and T. J. Weiler, Flavor Ratios of Astrophysical Neutrinos: Implications for Precision Measurements, *JHEP* **02**, 005, [arXiv:0711.4517](https://arxiv.org/abs/0711.4517) [[hep-ph](#)].
- [34] O. Mena, S. Palomares-Ruiz, and A. C. Vincent, Flavor Composition of the High-Energy Neutrino Events in IceCube, *Phys. Rev. Lett.* **113**, 091103 (2014), [arXiv:1404.0017](https://arxiv.org/abs/1404.0017) [[astro-ph.HE](#)].
- [35] S. Palomares-Ruiz, A. C. Vincent, and O. Mena, Spectral analysis of the high-energy IceCube neutrinos, *Phys. Rev. D* **91**, 103008 (2015), [arXiv:1502.02649](https://arxiv.org/abs/1502.02649) [[astro-ph.HE](#)].
- [36] M. Bustamante, J. F. Beacom, and W. Winter, Theoretically palatable flavor combinations of astrophysical neutrinos, *Phys. Rev. Lett.* **115**, 161302 (2015), [arXiv:1506.02645](https://arxiv.org/abs/1506.02645) [[astro-ph.HE](#)].
- [37] C. A. Argüelles, T. Katori, and J. Salvadó, New Physics in Astrophysical Neutrino Flavor, *Phys. Rev. Lett.* **115**, 161303 (2015), [arXiv:1506.02043](https://arxiv.org/abs/1506.02043) [[hep-ph](#)].
- [38] A. C. Vincent, S. Palomares-Ruiz, and O. Mena, Analysis of the 4-year IceCube high-energy starting events, *Phys. Rev. D* **94**, 023009 (2016), [arXiv:1605.01556](https://arxiv.org/abs/1605.01556) [[astro-ph.HE](#)].
- [39] V. Brdar, J. Kopp, and X.-P. Wang, Sterile Neutrinos and Flavor Ratios in IceCube, *JCAP* **01**, 026, [arXiv:1611.04598](https://arxiv.org/abs/1611.04598) [[hep-ph](#)].

- [40] M. Bustamante, J. F. Beacom, and K. Murase, Testing decay of astrophysical neutrinos with incomplete information, *Phys. Rev. D* **95**, 063013 (2017), [arXiv:1610.02096 \[astro-ph.HE\]](#).
- [41] R. W. Rasmussen, L. Lechner, M. Ackermann, M. Kowalski, and W. Winter, Astrophysical neutrinos flavored with Beyond the Standard Model physics, *Phys. Rev. D* **96**, 083018 (2017), [arXiv:1707.07684 \[hep-ph\]](#).
- [42] N. Klop and S. Ando, Effects of a neutrino-dark energy coupling on oscillations of high-energy neutrinos, *Phys. Rev. D* **97**, 063006 (2018), [arXiv:1712.05413 \[hep-ph\]](#).
- [43] Y. Farzan and S. Palomares-Ruiz, Flavor of cosmic neutrinos preserved by ultralight dark matter, *Phys. Rev. D* **99**, 051702 (2019), [arXiv:1810.00892 \[hep-ph\]](#).
- [44] M. Ahlers, M. Bustamante, and S. Mu, Unitarity Bounds of Astrophysical Neutrinos, *Phys. Rev. D* **98**, 123023 (2018), [arXiv:1810.00893 \[astro-ph.HE\]](#).
- [45] M. Bustamante and S. K. Agarwalla, Universe's Worth of Electrons to Probe Long-Range Interactions of High-Energy Astrophysical Neutrinos, *Phys. Rev. Lett.* **122**, 061103 (2019), [arXiv:1808.02042 \[astro-ph.HE\]](#).
- [46] C. A. Argüelles, K. Farrag, T. Katori, R. Khandelwal, S. Mandalia, and J. Salvadó, Sterile neutrinos in astrophysical neutrino flavor, *JCAP* **02**, 015, [arXiv:1909.05341 \[hep-ph\]](#).
- [47] M. Ahlers, M. Bustamante, and N. G. N. Willesen, Flavors of astrophysical neutrinos with active-sterile mixing, *JCAP* **07**, 029, [arXiv:2009.01253 \[hep-ph\]](#).
- [48] C. A. Argüelles and J. Salvadó, Sterile Neutrinos with Neutrino Telescopes, *Universe* **7**, 426 (2021), [arXiv:2111.03357 \[hep-ph\]](#).
- [49] K. Carloni, C. A. Argüelles, I. Martínez-Soler, K. S. Babu, and P. S. B. Dev, Probing Pseudo-Dirac Neutrinos with Astrophysical Sources at IceCube, *PoS ICRC2023*, 1040 (2023), [arXiv:2212.00737 \[astro-ph.HE\]](#).
- [50] B. Telalovic and M. Bustamante, Flavor Anisotropy in the High-Energy Astrophysical Neutrino Sky, (2023), [arXiv:2310.15224 \[astro-ph.HE\]](#).
- [51] M. G. Aartsen *et al.* (IceCube), A combined maximum-likelihood analysis of the high-energy astrophysical neutrino flux measured with IceCube, *Astrophys. J.* **809**, 98 (2015), [arXiv:1507.03991 \[astro-ph.HE\]](#).
- [52] M. Bustamante and M. Ahlers, Inferring the flavor of high-energy astrophysical neutrinos at their sources, *Phys. Rev. Lett.* **122**, 241101 (2019), [arXiv:1901.10087 \[astro-ph.HE\]](#).
- [53] A. D. Avrorin *et al.* (Baikal-GVD), Baikal-GVD: status and prospects, *EPJ Web Conf.* **191**, 01006 (2018), [arXiv:1808.10353 \[astro-ph.IM\]](#).
- [54] M. G. Aartsen *et al.* (IceCube-Gen2), IceCube-Gen2: the window to the extreme Universe, *J. Phys. G* **48**, 060501 (2021), [arXiv:2008.04323 \[astro-ph.HE\]](#).
- [55] S. Adrián-Martínez *et al.* (KM3Net), Letter of intent for KM3NeT 2.0, *J. Phys. G* **43**, 084001 (2016), [arXiv:1601.07459 \[astro-ph.IM\]](#).
- [56] M. Agostini *et al.* (P-ONE), The Pacific Ocean Neutrino Experiment, *Nature Astron.* **4**, 913 (2020), [arXiv:2005.09493 \[astro-ph.HE\]](#).
- [57] W. G. Thompson (TAMBO), TAMBO: Searching for Tau Neutrinos in the Peruvian Andes, in *38th International Cosmic Ray Conference* (2023) [arXiv:2308.09753 \[astro-ph.HE\]](#).
- [58] Z. P. Ye *et al.*, Proposal for a neutrino telescope in South China Sea, *Nature Astron.* [10.1038/s41550-023-02087-6](#) (2023), [arXiv:2207.04519 \[astro-ph.HE\]](#).
- [59] A. M. Hillas, The Origin of Ultrahigh-Energy Cosmic Rays, *Ann. Rev. Astron. Astrophys.* **22**, 425 (1984).
- [60] L. A. Anchordoqui, Ultra-High-Energy Cosmic Rays, *Phys. Rept.* **801**, 1 (2019), [arXiv:1807.09645 \[astro-ph.HE\]](#).
- [61] R. Alves Batista *et al.*, Open Questions in Cosmic-Ray Research at Ultrahigh Energies, *Front. Astron. Space Sci.* **6**, 23 (2019), [arXiv:1903.06714 \[astro-ph.HE\]](#).
- [62] S. H. Margolis, D. N. Schramm, and R. Silberberg, Ultrahigh-Energy Neutrino Astronomy, *Astrophys. J.* **221**, 990 (1978).
- [63] F. Stecker, Diffuse Fluxes of Cosmic High-Energy Neutrinos, *Astrophys. J.* **228**, 919 (1979).
- [64] S. Kelner, F. A. Aharonian, and V. Bugayov, Energy spectra of gamma-rays, electrons and neutrinos produced at proton-proton interactions in the very high energy regime, *Phys. Rev. D* **74**, 034018 (2006), [Erratum: *Phys. Rev. D* **79**, 039901 (2009)], [arXiv:astro-ph/0606058](#).
- [65] A. Mücke, R. Engel, J. Rachen, R. Protheroe, and T. Stanev, SOPHIA: Monte Carlo simulations of photohadronic processes in astrophysics, *Comput. Phys. Commun.* **124**, 290 (2000), [arXiv:astro-ph/9903478](#).
- [66] S. R. Kelner and F. A. Aharonian, Energy spectra of gamma-rays, electrons and neutrinos produced at interactions of relativistic protons with low energy radiation, *Phys. Rev. D* **78**, 034013 (2008), [Erratum: *Phys. Rev. D* **82**, 099901 (2010)], [arXiv:0803.0688 \[astro-ph\]](#).
- [67] S. Hümmer, M. Rüter, F. Spanier, and W. Winter, Simplified models for photohadronic interactions in cosmic accelerators, *Astrophys. J.* **721**, 630 (2010), [arXiv:1002.1310 \[astro-ph.HE\]](#).
- [68] L. Morejón, A. Fedynitch, D. Boncioli, D. Biehl, and W. Winter, Improved photomeson model for interactions of cosmic ray nuclei, *JCAP* **11**, 007, [arXiv:1904.07999 \[astro-ph.HE\]](#).
- [69] N. Song, S. Li, M. Bustamante, C. A. Argüelles, and A. Vincent, FANFIC: Future Astrophysical Neutrino Flavors In Contours, <https://github.com/songningqiang/FANFIC> (2021).
- [70] B. Abi *et al.* (DUNE), Deep Underground Neutrino Experiment (DUNE), Far Detector Technical Design Report, Volume I Introduction to DUNE, *JINST* **15** (08), T08008, [arXiv:2002.02967 \[physics.ins-det\]](#).
- [71] K. Abe *et al.* (Hyper-Kamiokande), Hyper-Kamiokande Design Report, (2018), [arXiv:1805.04163 \[physics.ins-det\]](#).
- [72] F. An *et al.* (JUNO), Neutrino Physics with JUNO, *J. Phys. G* **43**, 030401 (2016), [arXiv:1507.05613 \[physics.ins-det\]](#).
- [73] T. Kashti and E. Waxman, Flavoring astrophysical neutrinos: Flavor ratios depend on energy, *Phys. Rev. Lett.* **95**, 181101 (2005), [arXiv:astro-ph/0507599](#).
- [74] P. Lipari, M. Lusignoli, and D. Meloni, Flavor Composition and Energy Spectrum of Astrophysical Neutrinos, *Phys. Rev. D* **75**, 123005 (2007), [arXiv:0704.0718 \[astro-ph\]](#).
- [75] P. Baerwald, S. Hümmer, and W. Winter, Systematics in the Interpretation of Aggregated Neutrino Flux Limits and Flavor Ratios from Gamma-Ray Bursts, *As-*

- tro part. *Phys.* **35**, 508 (2012), arXiv:1107.5583 [astro-ph.HE].
- [76] M. Bustamante and I. Tamborra, Using high-energy neutrinos as cosmic magnetometers, *Phys. Rev. D* **102**, 123008 (2020), arXiv:2009.01306 [astro-ph.HE].
- [77] D. F. G. Fiorillo, A. Van Vliet, S. Morisi, and W. Winter, Unified thermal model for photohadronic neutrino production in astrophysical sources, *JCAP* **07**, 028, arXiv:2103.16577 [astro-ph.HE].
- [78] A. Bhattacharya, R. Enberg, M. H. Reno, and I. Sarcevic, Energy-dependent flavour ratios in neutrino telescopes from charm, (2023), arXiv:2309.09139 [astro-ph.HE].
- [79] K. Murase, S. S. Kimura, and P. Mészáros, Hidden Cores of Active Galactic Nuclei as the Origin of Medium-Energy Neutrinos: Critical Tests with the MeV Gamma-Ray Connection, *Phys. Rev. Lett.* **125**, 011101 (2020), arXiv:1904.04226 [astro-ph.HE].
- [80] K. Riabtsev and S. Troitsky, Energy-dependent flavor ratios, cascade/track spectrum tension and high-energy neutrinos from magnetospheres of supermassive black holes, *Phys. Lett. B* **839**, 137758 (2023), arXiv:2204.09339 [astro-ph.HE].
- [81] J. F. Beacom, N. F. Bell, D. Hooper, S. Pakvasa, and T. J. Weiler, Decay of High-Energy Astrophysical Neutrinos, *Phys. Rev. Lett.* **90**, 181301 (2003), arXiv:hep-ph/0211305.
- [82] P. Mehta and W. Winter, Interplay of energy dependent astrophysical neutrino flavor ratios and new physics effects, *JCAP* **03**, 041, arXiv:1101.2673 [hep-ph].
- [83] P. Baerwald, M. Bustamante, and W. Winter, Neutrino Decays over Cosmological Distances and the Implications for Neutrino Telescopes, *JCAP* **10**, 020, arXiv:1208.4600 [astro-ph.CO].
- [84] I. M. Shoemaker and K. Murase, Probing BSM Neutrino Physics with Flavor and Spectral Distortions: Prospects for Future High-Energy Neutrino Telescopes, *Phys. Rev. D* **93**, 085004 (2016), arXiv:1512.07228 [astro-ph.HE].
- [85] P. B. Denton and I. Tamborra, Invisible Neutrino Decay Could Resolve IceCube's Track and Cascade Tension, *Phys. Rev. Lett.* **121**, 121802 (2018), arXiv:1805.05950 [hep-ph].
- [86] M. Bustamante, New limits on neutrino decay from the Glashow resonance of high-energy cosmic neutrinos, (2020), arXiv:2004.06844 [astro-ph.HE].
- [87] A. Abdullahi and P. B. Denton, Visible Decay of Astrophysical Neutrinos at IceCube, *Phys. Rev. D* **102**, 023018 (2020), arXiv:2005.07200 [hep-ph].
- [88] G. Barenboim and C. Quigg, Neutrino observatories can characterize cosmic sources and neutrino properties, *Phys. Rev. D* **67**, 073024 (2003), arXiv:hep-ph/0301220.
- [89] M. Bustamante, A. M. Gago, and C. Peña-Garay, Energy-Independent New Physics in the Flavour Ratios of High-Energy Astrophysical Neutrinos, *JHEP* **04**, 066, arXiv:1001.4878 [hep-ph].
- [90] C. A. Argüelles and T. Katori, Lorentz Symmetry and High-Energy Neutrino Astronomy, *Universe* **7**, 490 (2021), arXiv:2109.13973 [hep-ph].
- [91] F. Testagrossa, D. F. G. Fiorillo, and M. Bustamante, Two-detector flavor sensitivity to ultra-high-energy cosmic neutrinos, (2023), arXiv:2310.12215 [astro-ph.HE].
- [92] S. Karmakar, S. Pandey, and S. Rakshit, Astronomy with energy dependent flavour ratios of extragalactic neutrinos, *JHEP* **10**, 004, arXiv:2010.07336 [hep-ph].
- [93] C. A. Argüelles, K. Farrag, and T. Katori, Ultra-light Dark Matter Limits from Astrophysical Neutrino Flavour, *PoS ICRC2023*, 1415 (2023).
- [94] D. F. G. Fiorillo, S. Morisi, G. Miele, and N. Saviano, Observable features in ultrahigh energy neutrinos due to active-sterile secret interactions, *Phys. Rev. D* **102**, 083014 (2020), arXiv:2007.07866 [hep-ph].
- [95] J. M. Berryman *et al.*, Neutrino self-interactions: A white paper, *Phys. Dark Univ.* **42**, 101267 (2023), arXiv:2203.01955 [hep-ph].
- [96] S. K. Agarwalla, M. Bustamante, S. Das, and A. Narang, Present and future constraints on flavor-dependent long-range interactions of high-energy astrophysical neutrinos, *JHEP* **08**, 113, arXiv:2305.03675 [hep-ph].
- [97] J. F. Beacom, N. F. Bell, D. Hooper, J. G. Learned, S. Pakvasa, and T. J. Weiler, PseudoDirac neutrinos: A Challenge for neutrino telescopes, *Phys. Rev. Lett.* **92**, 011101 (2004), arXiv:hep-ph/0307151.
- [98] T. Rink and M. Sen, Constraints on pseudo-Dirac neutrinos using high-energy neutrinos from NGC 1068, (2022), arXiv:2211.16520 [hep-ph].
- [99] M. Bustamante, A. M. Gago, and J. Jones Pérez, SUSY Renormalization Group Effects in Ultra High Energy Neutrinos, *JHEP* **05**, 133, arXiv:1012.2728 [hep-ph].
- [100] H. Minakata and A. Y. Smirnov, High-energy cosmic neutrinos and the equivalence principle, *Phys. Rev. D* **54**, 3698 (1996), arXiv:hep-ph/9601311.
- [101] D. F. G. Fiorillo, G. Mangano, S. Morisi, and O. Pisanti, IceCube constraints on violation of equivalence principle, *JCAP* **04**, 079, arXiv:2012.07867 [hep-ph].
- [102] A. Esmaili, Violation of Equivalence Principle in Neutrino Sector: Probing the Extended Parameter Space, *JCAP* **07**, 018, arXiv:2105.08744 [hep-ph].
- [103] M. Chianese, D. F. G. Fiorillo, G. Mangano, G. Miele, S. Morisi, and O. Pisanti, Sensitivity of KM3NeT to Violation of Equivalence Principle, *Symmetry* **13**, 1353 (2021), arXiv:2107.13013 [hep-ph].
- [104] M. G. Aartsen *et al.* (IceCube), Measurement of the multi-TeV neutrino cross section with IceCube using Earth absorption, *Nature* **551**, 596 (2017), arXiv:1711.08119 [hep-ex].
- [105] M. Bustamante and A. Connolly, Extracting the Energy-Dependent Neutrino-Nucleon Cross Section above 10 TeV Using IceCube Showers, *Phys. Rev. Lett.* **122**, 041101 (2019), arXiv:1711.11043 [astro-ph.HE].
- [106] M. Aartsen *et al.* (IceCube), Measurements using the inelasticity distribution of multi-TeV neutrino interactions in IceCube, *Phys. Rev. D* **99**, 032004 (2019), arXiv:1808.07629 [hep-ex].
- [107] R. Abbasi *et al.* (IceCube), Measurement of the high-energy all-flavor neutrino-nucleon cross section with IceCube, *Phys. Rev. D* **104**, 022001 (2021), arXiv:2011.03560 [hep-ex].
- [108] S. W. Barwick and C. Glaser, Chapter 6: Radio Detection of High Energy Neutrinos in Ice, , 237 (2023), arXiv:2208.04971 [astro-ph.IM].
- [109] Z. Yao, M. Chen, and J. Liu, Progress on LHAASO and high-energy neutrino telescope (2023), Symposium on frontiers of underground and space particle physics and cosmophysics.
- [110] T.-Q. Huang, Z. Cao, M. Chen, J. Liu, Z. Wang, X. You, and Y. Qi, Proposal for the High Energy Neutrino Telescope, *PoS ICRC2023*, 1080 (2023).

- [111] D. F. G. Fiorillo and M. Bustamante, Bump hunting in the diffuse flux of high-energy cosmic neutrinos, *Phys. Rev. D* **107**, 083008 (2023), arXiv:2301.00024 [astro-ph.HE].
- [112] Q. Liu, N. Song, and A. C. Vincent, Probing neutrino production in high-energy astrophysical neutrino sources with the Glashow resonance, *Phys. Rev. D* **108**, 043022 (2023), arXiv:2304.06068 [astro-ph.HE].
- [113] M. Aartsen *et al.* (IceCube), The IceCube Neutrino Observatory: Instrumentation and Online Systems, *JINST* **12** (03), P03012, arXiv:1612.05093 [astro-ph.IM].
- [114] M. G. Aartsen *et al.* (IceCube), Neutrino astronomy with the next generation IceCube Neutrino Observatory, (2019), arXiv:1911.02561 [astro-ph.HE].
- [115] G. Safronov (Baikal-GVD), Baikal-GVD: status and first results, in *40th International Conference on High Energy Physics* (2020) arXiv:2012.03373 [astro-ph.HE].
- [116] V. A. Allakhverdyan *et al.* (Baikal-GVD), High-energy neutrino-induced cascade from the direction of the flaring radio blazar TXS 0506+056 observed by the Baikal Gigaton Volume Detector in 2021, (2022), arXiv:2210.01650 [astro-ph.HE].
- [117] V. A. Allakhverdyan *et al.* (Baikal-GVD), Diffuse neutrino flux measurements with the Baikal-GVD neutrino telescope, *Phys. Rev. D* **107**, 042005 (2023), arXiv:2211.09447 [astro-ph.HE].
- [118] M. Agostini *et al.* (P-ONE), The Pacific Ocean Neutrino Experiment, *Nature Astron.* **4**, 913 (2020), arXiv:2005.09493 [astro-ph.HE].
- [119] A. Romero-Wolf *et al.*, An Andean Deep-Valley Detector for High-Energy Tau Neutrinos, in *Latin American Strategy Forum for Research Infrastructure* (2020) arXiv:2002.06475 [astro-ph.IM].
- [120] R. L. Workman *et al.* (Particle Data Group), Review of Particle Physics, *PTEP* **2022**, 083C01 (2022).
- [121] S. L. Glashow, Resonant Scattering of Antineutrinos, *Phys. Rev.* **118**, 316 (1960).
- [122] M. G. Aartsen *et al.* (IceCube), Detection of a particle shower at the Glashow resonance with IceCube, *Nature* **591**, 220 (2021), [Erratum: Nature 592, E11 (2021)], arXiv:2110.15051 [hep-ex].
- [123] D. Biehl, A. Fedynitch, A. Palladino, T. J. Weiler, and W. Winter, Astrophysical Neutrino Production Diagnostics with the Glashow Resonance, *JCAP* **01**, 033, arXiv:1611.07983 [astro-ph.HE].
- [124] G.-y. Huang and Q. Liu, Hunting the Glashow Resonance with PeV Neutrino Telescopes, *JCAP* **03**, 005, arXiv:1912.02976 [hep-ph].
- [125] G.-y. Huang, M. Lindner, and N. Volmer, Inferring astrophysical neutrino sources from the Glashow resonance, *JHEP* **11** (1), 164, arXiv:2303.13706 [hep-ph].
- [126] M. G. Aartsen *et al.* (IceCube), Flavor Ratio of Astrophysical Neutrinos above 35 TeV in IceCube, *Phys. Rev. Lett.* **114**, 171102 (2015), arXiv:1502.03376 [astro-ph.HE].
- [127] R. Abbasi *et al.* (IceCube), Improved Characterization of the Astrophysical Muon-neutrino Flux with 9.5 Years of IceCube Data, *Astrophys. J.* **928**, 50 (2022), arXiv:2111.10299 [astro-ph.HE].
- [128] R. Naab, E. Ganster, and Z. Zhang (IceCube), Measurement of the astrophysical diffuse neutrino flux in a combined fit of IceCube's high energy neutrino data, in *38th International Cosmic Ray Conference* (2023) arXiv:2308.00191 [astro-ph.HE].
- [129] L. J. Schumacher, M. Huber, M. Agostini, M. Bustamante, F. Oikonomou, and E. Resconi, PLEνM: A global and distributed monitoring system of high-energy astrophysical neutrinos, *PoS ICRC2021*, 1185 (2021), arXiv:2107.13534 [astro-ph.IM].
- [130] N. Haba and H. Murayama, Anarchy and hierarchy, *Phys. Rev. D* **63**, 053010 (2001), arXiv:hep-ph/0009174.
- [131] C. A. Argüelles, A. Schneider, and T. Yuan, A binned likelihood for stochastic models, *JHEP* **06**, 030, arXiv:1901.04645 [physics.data-an].
- [132] Mceq, <https://github.com/mceq-project/MCEq>.
- [133] J. M. Picone, A. E. Hedin, D. P. Drob, and A. C. Aikin, NRLMSISE-00 empirical model of the atmosphere: Statistical comparisons and scientific issues, *Journal of Geophysical Research: Space Physics* **107**, SIA (2002).
- [134] T. K. Gaisser, Spectrum of cosmic-ray nucleons, kaon production, and the atmospheric muon charge ratio, *Astropart. Phys.* **35**, 801 (2012), arXiv:1111.6675 [astro-ph.HE].
- [135] F. Riehn, H. P. Dembinski, R. Engel, A. Fedynitch, T. K. Gaisser, and T. Stanev, The hadronic interaction model SIBYLL 2.3c and Feynman scaling, *PoS ICRC2017*, 301 (2018), arXiv:1709.07227 [hep-ph].
- [136] R. Abbasi *et al.* (IceCube), IceCube Data for Neutrino Point-Source Searches Years 2008-2018 10.21234/CPKQ-K003 (2021), arXiv:2101.09836 [astro-ph.HE].
- [137] J. Buchner, A statistical test for Nested Sampling algorithms, *Statistics and Computing* **26**, 383 (2016), arXiv:1407.5459 [stat.CO].
- [138] J. Buchner, Collaborative Nested Sampling: Big Data vs. complex physical models, *Publications of the Astronomical Society of the Pacific* **131**, 108005 (2019), arXiv:1707.04476 [stat.CO].
- [139] J. Buchner, UltraNest — a robust, general purpose Bayesian inference engine, *The Journal of Open Source Software* **6**, 3001 (2021), arXiv:2101.09604 [stat.CO].
- [140] H. Jeffreys, *The Theory of Probability*, Oxford Classic Texts in the Physical Sciences (OUP Oxford, 1998).
- [141] V. Basu *et al.* (IceCube), From PeV to TeV: Astrophysical Neutrinos with Contained Vertices in 10 years of IceCube Data, *PoS ICRC2023*, 1007 (2023), arXiv:2307.15183 [astro-ph.HE].
- [142] M. Huenefeld *et al.* (IceCube), Combining Maximum-Likelihood with Deep Learning for Event Reconstruction in IceCube, *PoS ICRC2021*, 1065 (2021), arXiv:2107.12110 [astro-ph.HE].
- [143] R. Abbasi *et al.* (IceCube), Graph Neural Networks for low-energy event classification & reconstruction in IceCube, *JINST* **17** (11), P11003, arXiv:2209.03042 [hep-ex].
- [144] R. Abbasi *et al.* (IceCube), Observation of high-energy neutrinos from the Galactic plane, *Science* **380**, adc9818 (2023), arXiv:2307.04427 [astro-ph.HE].
- [145] R. Abbasi *et al.* (IceCube), Summary of IceCube tau neutrino searches and flavor composition measurements of the diffuse astrophysical neutrino flux, *PoS ICRC2023*, 1122 (2023), arXiv:2308.15213 [astro-ph.HE].
- [146] S. W. Li, M. Bustamante, and J. F. Beacom, Echo Technique to Distinguish Flavors of Astrophysical Neutrinos, *Phys. Rev. Lett.* **122**, 151101 (2019), arXiv:1606.06290 [astro-ph.HE].

- [147] A. Steuer and L. Köpke (IceCube), Delayed light emission to distinguish astrophysical neutrino flavors in IceCube, *PoS ICRC2017*, 1008 (2018).
- [148] K. Farrag *et al.*, Distinguishing ν_τ neutrinos using the neutron echo technique with next generation ice Cherenkov telescopes, *PoS ICRC2023*, 1211 (2023).

Appendix A: Posterior distributions and allowed intervals of the model parameters

In Section IV in the main text, we describe how we compute the joint posterior probability of the free model parameters (Table II) that we use to measure the flavor composition at Earth, $f_{\alpha,\oplus}^{\text{LE}}$ and $f_{\alpha,\oplus}^{\text{HE}}$, and infer the flavor composition at the sources, $f_{\alpha,S}^{\text{LE}}$ and $f_{\alpha,S}^{\text{HE}}$. In the main text, we show posteriors of the flavor composition, marginalized over all the other model parameters (Figs. 1, 3, and 7).

To complement those results, and for the purpose of illustration, below we show joint two-dimensional pairwise posteriors for all the model parameters for our present and projected results for the year 2040. For our projections, we fix the transition energy to $E_{\text{trans}} = 1$ PeV. (We have also generated projections assuming $E_{\text{trans}} = 200$ TeV, and for other years, but we do not show the joint posteriors for those cases.)

Figures A1–A3 show posteriors for the measurement

of the flavor composition at Earth for our PL, BPL, and Step benchmark flux models.

Figures A4–A6 show posteriors for the inferred flavor composition at the sources for our PL, BPL, and Step benchmark flux models.

Figures A1–A6 confirm that there are appreciable correlations between the flavor fractions; this is shown already in Figs. 1, 3, and 7 in the main text. The figures also reveal that the parameters that determine the shape of the neutrino spectrum (Table II)—the flux normalization factors, spectral indices, and transition energy—are only weakly correlated with the flavor fractions, especially in our projections. This lends support to our finding (Section V) that the evidence for the existence of a transition in energy stems largely from a change in the spectrum shape.

Table A1 shows the best-fit values of the flavor composition measured at Earth, $f_{\alpha,\oplus}^{\text{LE}}$ and $f_{\alpha,\oplus}^{\text{HE}}$, and the allowed ranges of the transition energy, for each of our benchmark flux models. For the flavor composition, given the significant correlations between the flavor fractions, instead of showing one-dimensional marginalized results, we refer to their joint two-dimensional allowed regions in Figs. A1–A3, and Figs. 1 and 3 in the main text.

Table A2 shows the allowed ranges of the inferred flavor composition at the sources, $f_{e,S}^{\text{LE}}$ and $f_{e,S}^{\text{HE}}$, and of the transition energy, for each of our benchmark flux models.

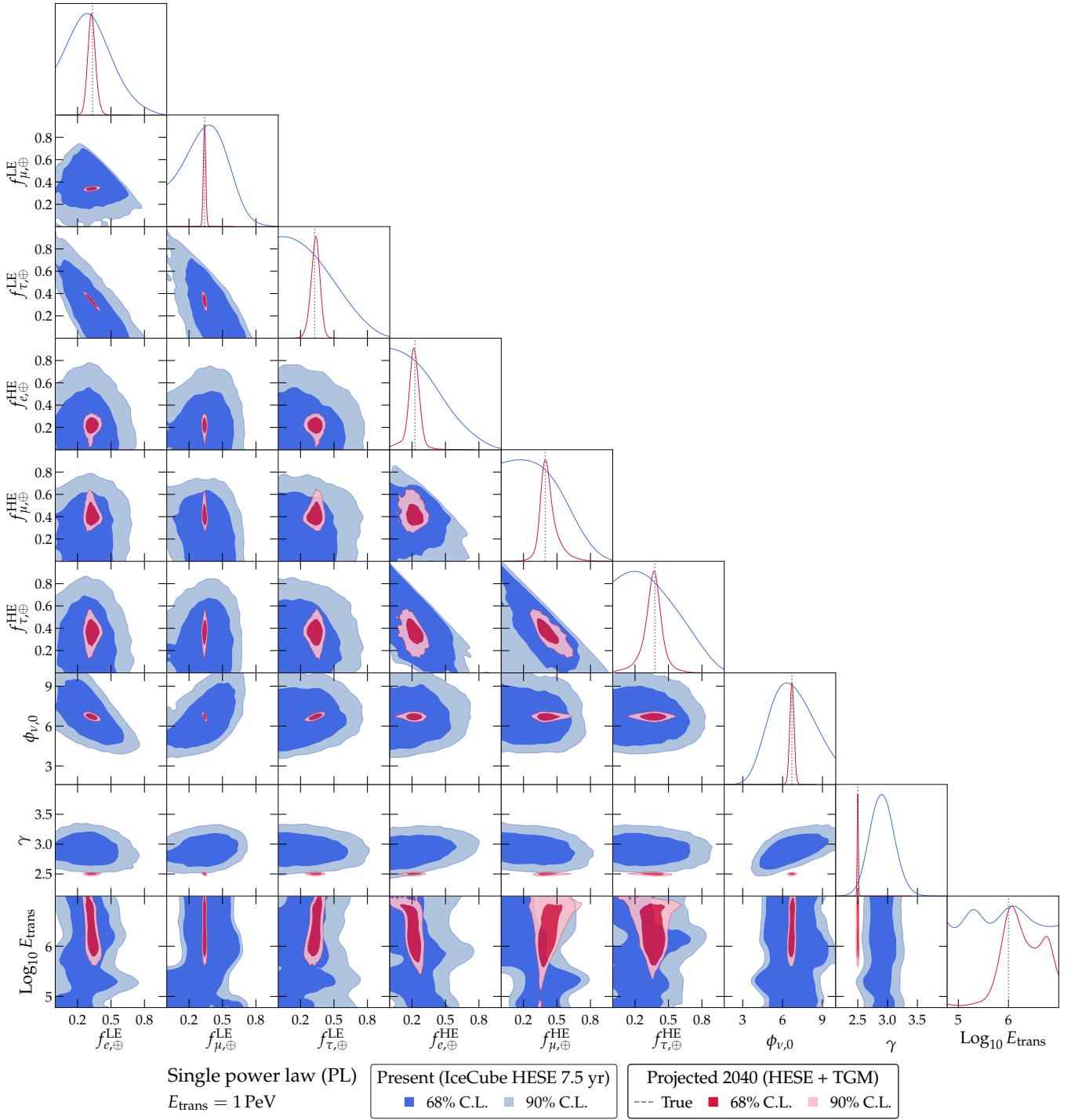


FIG. A1. *Joint posterior distributions of the model parameters in the measurement of the flavor composition at Earth, for the power law (PL) benchmark neutrino spectrum.* See Table II for a description of the parameters, including units, and Fig. 2 for the specific PL flux that we use to make our projections. The full joint posterior is Eq. (14) in the main text. Each panel shows the two-dimensional posterior marginalized over all model parameters except for the two in the panel. Allowed regions are for 68% and 90% C.L.. In this figure (and also in Figs. A2 and A3), we fix the true value of the transition energy in our projections to $E_{\text{trans}} = 1 \text{ PeV}$. See Table A1 for best-fit values and one-dimensional allowed intervals of selected parameters. Section V A in the main text for details.

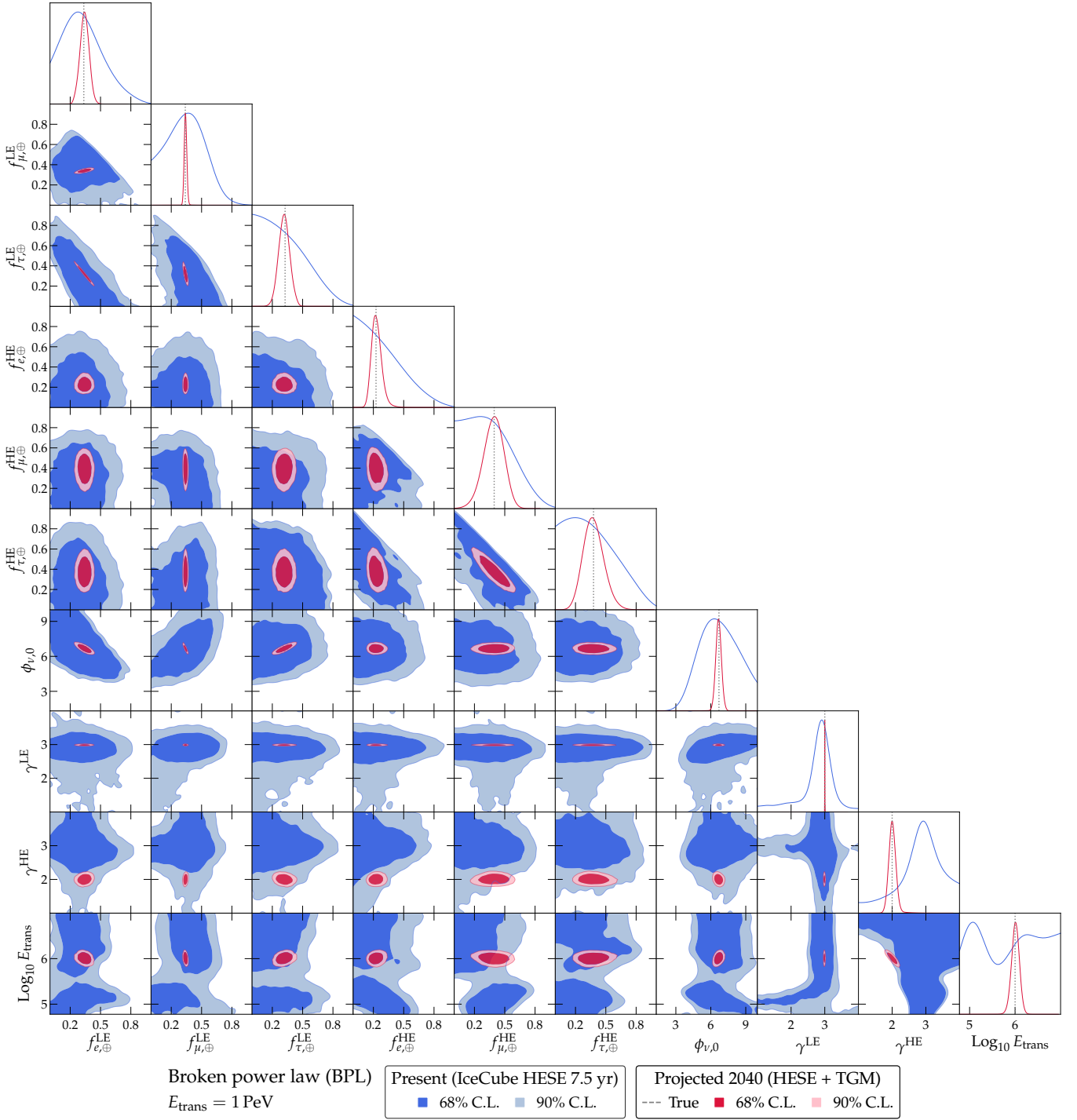


FIG. A2. *Joint posterior distributions of the model parameters in the measurement of the flavor composition at Earth, for the broken power law (BPL) benchmark neutrino spectrum. Same as Fig. A1, but for the BPL flux.*

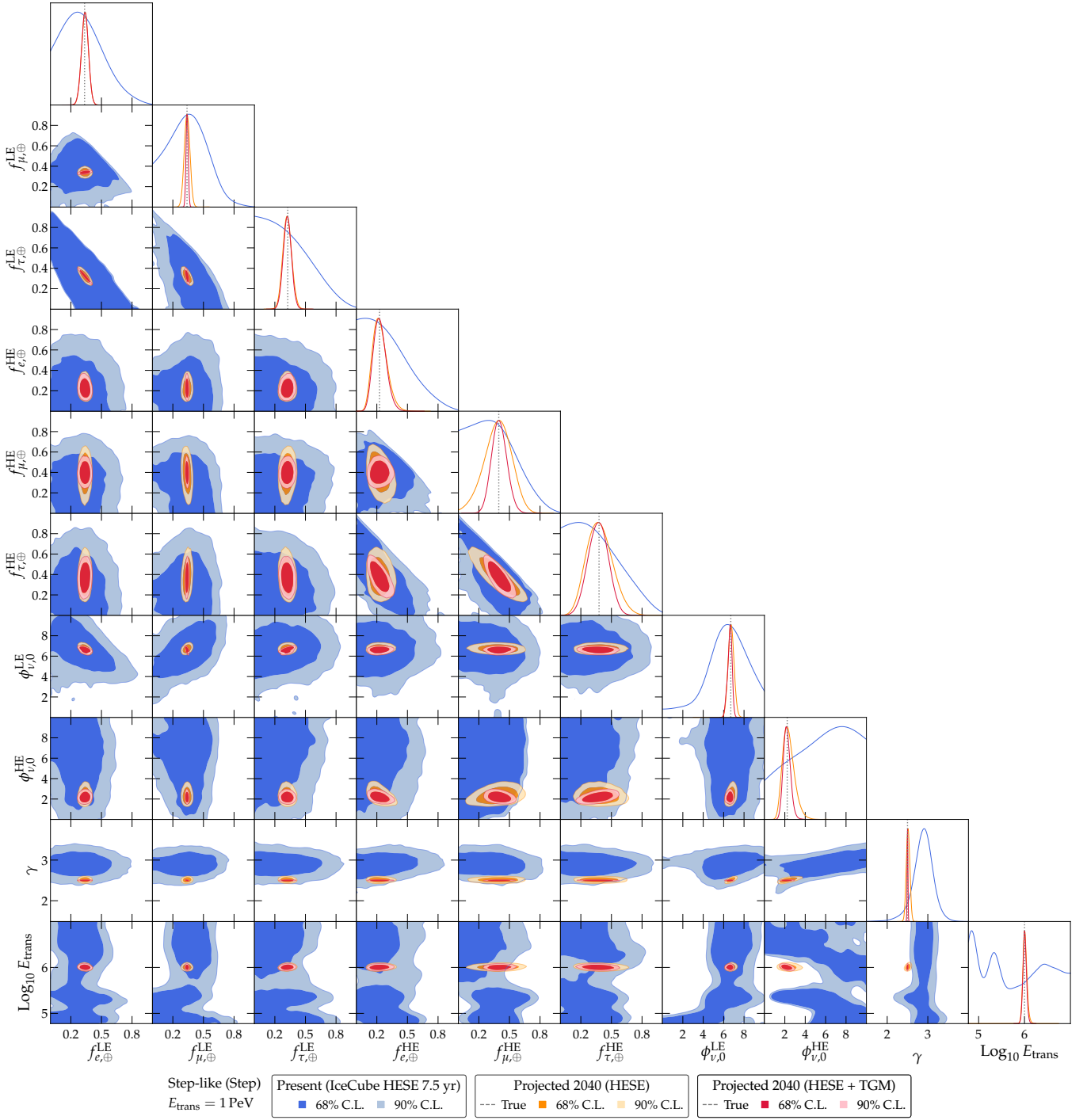


FIG. A3. *Joint posterior distributions of the model parameters in the measurement of the flavor composition at Earth, for the step-like (Step) benchmark neutrino spectrum.* Same as Fig. A1, but for the Step flux. Furthermore, the projection for 2040 with HESE-only selection is shown as orange regions, where the improvement from the inclusion of TGM can be seen compared to the red regions.

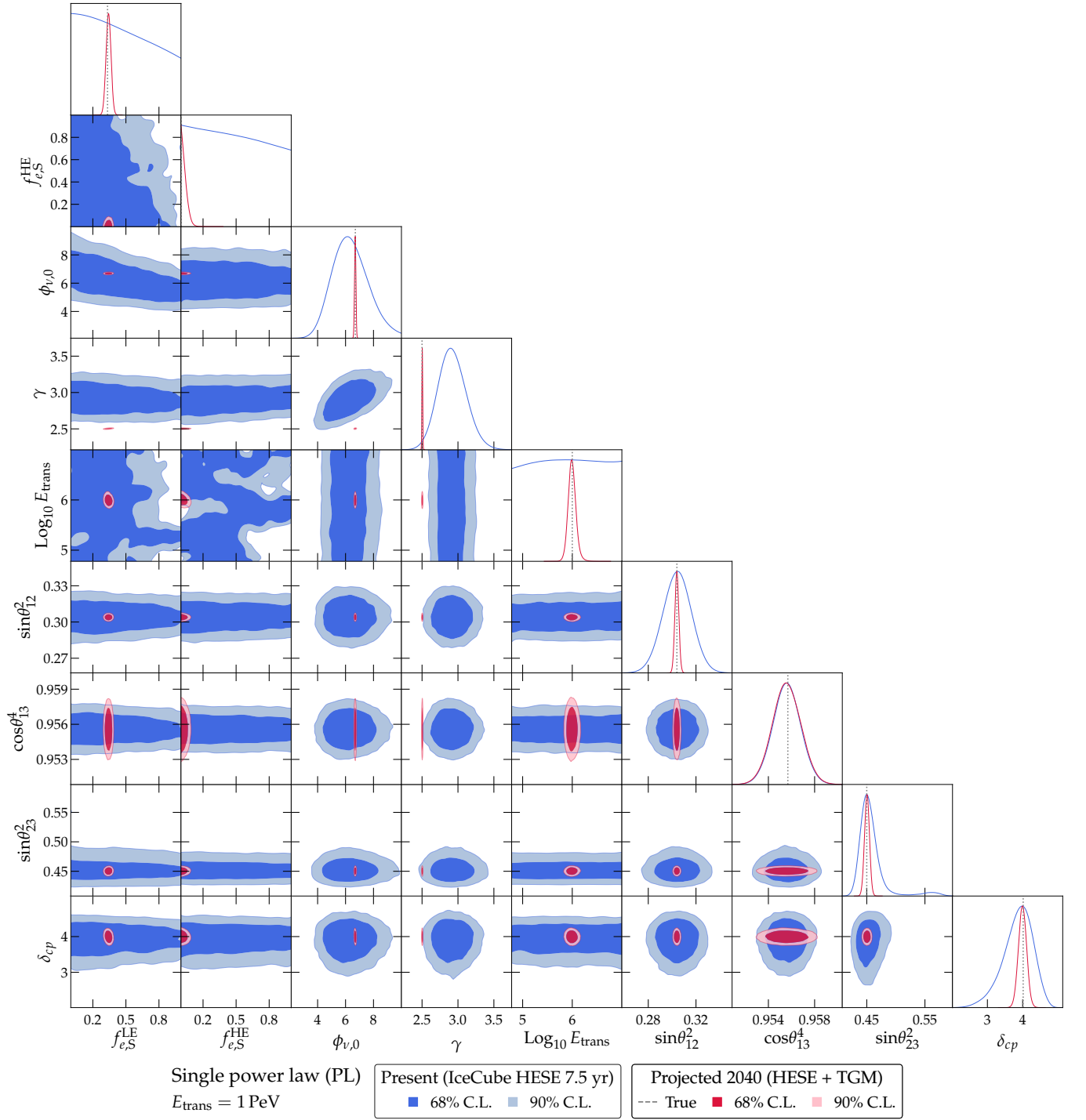


FIG. A4. *Joint posterior distributions of the model parameters inferring the flavor composition at sources, for the power law (PL) benchmark neutrino spectrum.* See Table II for a description of the parameters, including units, and Fig. 2 for the specific PL flux that we use to make our projections. The full joint posterior is Eq. (14) in the main text. Each panel shows the two-dimensional posterior marginalized over all model parameters except for the two in the panel. Allowed regions are for 68% and 90% C.L.. In this figure (and also in Figs. A5 and A6), we fix the true value of the transition energy in our projections to $E_{\text{trans}} = 1$ PeV. See Table A2 for best-fit values and one-dimensional allowed intervals of selected parameters. See Section VC in the main text for details.

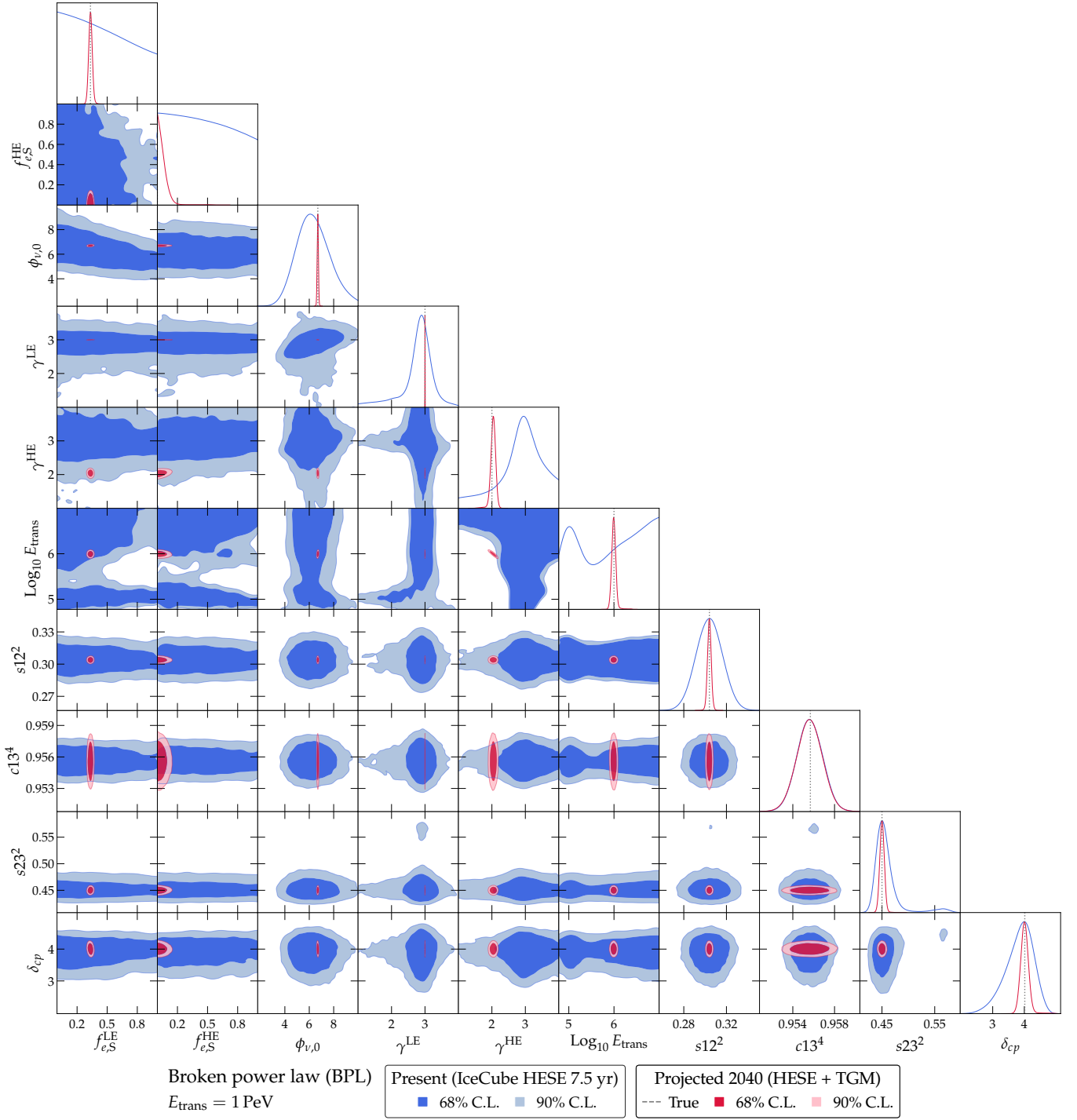


FIG. A5. *Joint posterior distributions of the model parameters inferring the flavor composition at sources, for the broken power law (BPL) benchmark neutrino spectrum. Same as Fig. A4, but for the BPL flux.*

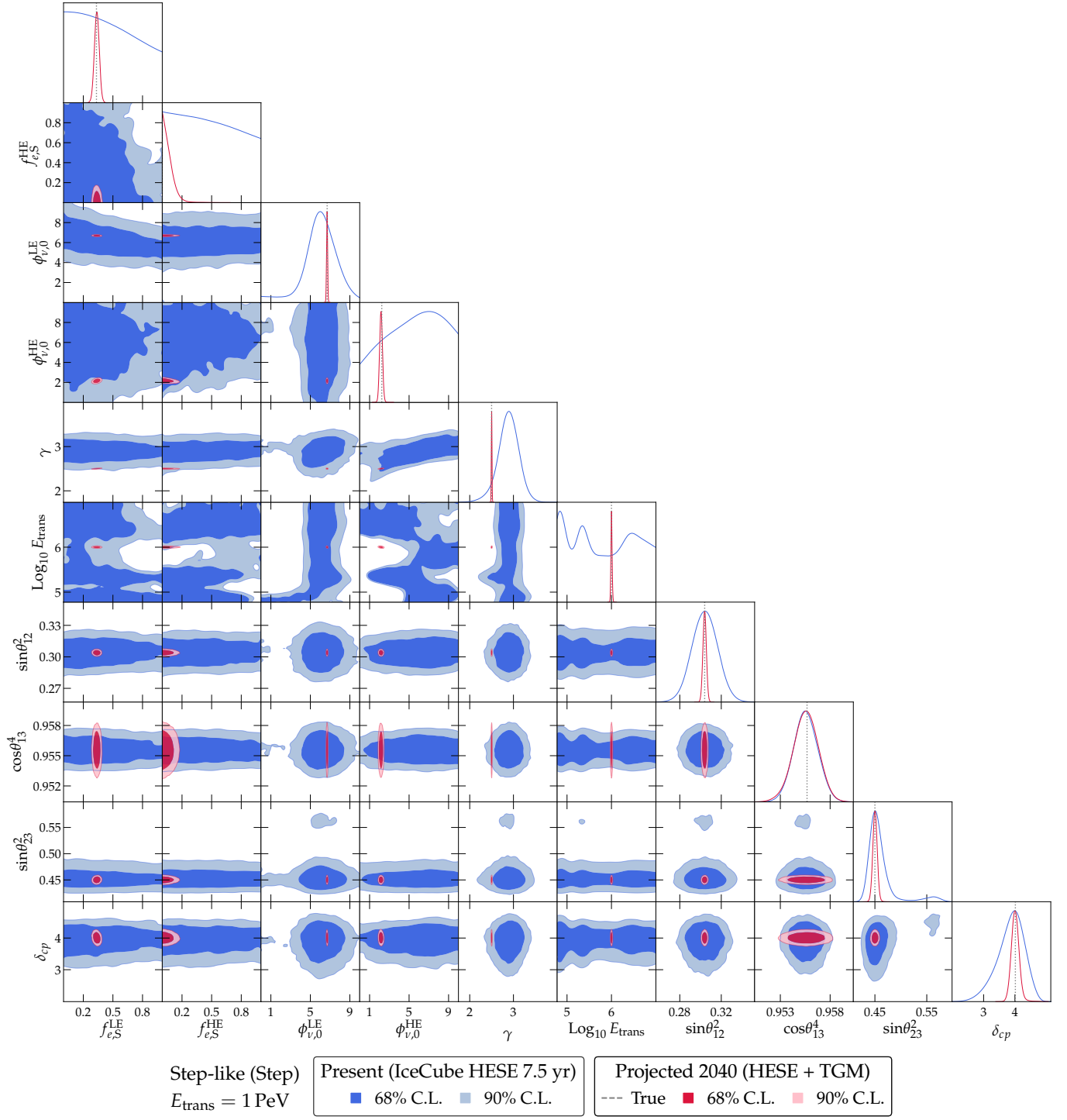


FIG. A6. *Joint posterior distributions of the model parameters inferring the flavor composition at sources, for the step-like (Step) benchmark neutrino spectrum. Same as Fig. A4, but for the Step flux.*

TABLE A1. *Flavor composition of high-energy astrophysical neutrinos at Earth, measured from fits to present IceCube data and projected data.* Present measurements are from the public IceCube 7.5-year HESE sample [16, 17] (Section IV C). Forecasts are from the combined, cumulative detection of HESE and TGM (Sections IV D and IV E) in the year 2040 by IceCube and future neutrino telescopes Baikal-GVD, IceCube-Gen2, KM3NeT, P-ONE, TAMBO, and TRIDENT (Section III). The flavor composition is measured separately for our three benchmark neutrino spectra (Section II A)—power law (PL), broken power law (BPL), and step-like (Step)—using the methods in Section IV A, with the priors from Table II. We have converted the flavor angles that are varied in the fit (Table II) into the flavor fractions at LE, $f_{\alpha,\oplus}^{\text{LE}}$ ($\alpha = e, \mu, \tau$), and high energies, $f_{\alpha,\oplus}^{\text{HE}}$; the conversion is in Section IV A. For each parameter, its allowed range is the one-dimensional 68% C.L. obtained by marginalizing the multi-dimensional posterior, Eq. (14), over all other parameters. See Section V A for details.

Flux model	Present (IceCube, HESE 7.5 yr)			Projected 2040 (multiple detectors, HESE + TGM)			
	E_{trans} [TeV]	Flavor composition at Earth (best fit) ^a		E_{trans} [TeV]		Flavor composition at Earth (best fit) ^a	
		LE ($< E_{\text{trans}}$) ($f_{e,\oplus}^{\text{LE}}, f_{\mu,\oplus}^{\text{LE}}, f_{\tau,\oplus}^{\text{LE}}$)	HE ($> E_{\text{trans}}$) ($f_{e,\oplus}^{\text{HE}}, f_{\mu,\oplus}^{\text{HE}}, f_{\tau,\oplus}^{\text{HE}}$)	True	Measured	LE ($< E_{\text{trans}}$) ($f_{e,\oplus}^{\text{LE}}, f_{\mu,\oplus}^{\text{LE}}, f_{\tau,\oplus}^{\text{LE}}$)	HE ($> E_{\text{trans}}$) ($f_{e,\oplus}^{\text{HE}}, f_{\mu,\oplus}^{\text{HE}}, f_{\tau,\oplus}^{\text{HE}}$)
PL	$192.63^{+2776.91}_{-87.41}$	(0.28, 0.35, 0.37)	(0.24, 0.32, 0.44)	200	$197.69^{+104.54}_{-51.06}$	(0.31, 0.33, 0.36)	(0.22, 0.40, 0.38)
				10^3	$893.32^{+3068.38}_{-396.29}$	(0.32, 0.34, 0.34)	(0.21, 0.41, 0.38)
BPL	$115.83^{+2205.10}_{-48.78}$	(0.22, 0.29, 0.49)	(0.12, 0.27, 0.61)	200	$190.95^{+16.50}_{-12.47}$	(0.35, 0.33, 0.32)	(0.22, 0.40, 0.38)
				10^3	$955.53^{+255.22}_{-132.49}$	(0.34, 0.32, 0.34)	(0.21, 0.39, 0.40)
Step	$78.85^{+2066.11}_{-15.83}$	(0.24, 0.34, 0.42)	(0.25, 0.32, 0.43)	200	$198.57^{+9.24}_{-9.91}$	(0.33, 0.31, 0.36)	(0.21, 0.39, 0.40)
				10^3	$985.33^{+124.21}_{-62.98}$	(0.34, 0.34, 0.32)	(0.24, 0.41, 0.35)

^a We show only the best-fit values of the flavor composition because the flavor fractions are highly correlated. We refer instead to their two-dimension allowed ranges in Figs. A1–A3, and Figs. 1 and 3 in the main text.

TABLE A2. *Flavor composition of high-energy astrophysical neutrinos at the sources, inferred from fits to present IceCube data and projected data.* We assume no ν_τ production in the sources, *i.e.*, $f_{\tau,S}^{\text{LE}} = f_{\tau,S}^{\text{HE}} = 0$, so we only need to infer the ν_e fractions, $f_{e,S}^{\text{LE}}$ and $f_{e,S}^{\text{HE}}$; the ν_μ fractions are $f_{\mu,S}^{\text{LE}} = 1 - f_{e,S}^{\text{LE}}$ and $f_{\mu,S}^{\text{HE}} = 1 - f_{e,S}^{\text{HE}}$. Present measurements are from the public IceCube 7.5-year HESE sample [16, 17] (Section IV C) and use present uncertainties on neutrino mixing parameters from NuFIT 5.1 [20, 21], (Table II). Forecasts are from the combined, cumulative detection of HESE and TGM (Sections IV D and IV E) in the year 2040 by IceCube and future neutrino telescopes Baikal-GVD, IceCube-Gen2, KM3NeT, P-ONE, TAMBO, and TRIDENT (Section III), and assume improved measurements of the mixing parameters by DUNE, Hyper-Kamiokande, and JUNO (Table II). The flavor composition is measured separately for our three benchmark neutrino spectra (Section II A)—power law (PL), broken power law (BPL), and step-like (Step)—using the methods in Section IV A, with the priors from Table II. For each parameter, its allowed range is the one-dimensional 68% C.L. obtained by marginalizing the multi-dimensional posterior, Eq. (14), over all other parameters. See Section V C for details.

Flux model	Present (IceCube, HESE 7.5 yr)			Projected 2040 (multiple detectors, HESE + TGM)			
	E_{trans} [TeV]	Flavor composition at sources ^a		E_{trans} [TeV]		Flavor composition at sources ^a	
		LE ($< E_{\text{trans}}$) ($f_{e,S}^{\text{LE}}, f_{\mu,S}^{\text{LE}}, f_{\tau,S}^{\text{LE}}$)	HE ($> E_{\text{trans}}$) ($f_{e,S}^{\text{HE}}, f_{\mu,S}^{\text{HE}}, f_{\tau,S}^{\text{HE}}$)	True	Measured	LE ($< E_{\text{trans}}$) ($f_{e,S}^{\text{LE}}, f_{\mu,S}^{\text{LE}}, f_{\tau,S}^{\text{LE}}$)	HE ($> E_{\text{trans}}$) ($f_{e,S}^{\text{HE}}, f_{\mu,S}^{\text{HE}}, f_{\tau,S}^{\text{HE}}$)
PL	$8317.64^{+1454.73}_{-8001.41}$	($0.06^{+0.57}_{-0.05}, 0.94^{+0.05}_{-0.57}, 0$)	($0.21^{+0.47}_{-0.18}, 0.79^{+0.18}_{-0.47}, 0$)	200	$199.53^{+24.35}_{-17.56}$	($0.34^{+0.03}_{-0.03}, 0.66^{+0.03}_{-0.03}, 0$)	($0.00^{+0.03}_{-0.00}, 1.00^{+0.00}_{-0.03}, 0$)
				10^3	$933.25^{+241.64}_{-101.49}$	($0.34^{+0.02}_{-0.02}, 0.66^{+0.02}_{-0.02}, 0$)	($0.00^{+0.04}_{-0.00}, 1.00^{+0.00}_{-0.04}, 0$)
BPL	$97.72^{+3138.21}_{-20.10}$	($0.19^{+0.43}_{-0.18}, 0.81^{+0.18}_{-0.43}, 0$)	($0.02^{+0.64}_{-0.00}, 0.98^{+0.00}_{-0.64}, 0$)	200	$199.53^{+4.65}_{-4.54}$	($0.34^{+0.04}_{-0.04}, 0.66^{+0.04}_{-0.04}, 0$)	($0.00^{+0.05}_{-0.00}, 1.00^{+0.00}_{-0.05}, 0$)
				10^3	$1000.00^{+96.48}_{-108.75}$	($0.34^{+0.02}_{-0.02}, 0.66^{+0.02}_{-0.02}, 0$)	($0.00^{+0.07}_{-0.00}, 1.00^{+0.00}_{-0.07}, 0$)
Step	$79.43^{+2009.86}_{-19.18}$	($0.22^{+0.43}_{-0.18}, 0.78^{+0.18}_{-0.43}, 0$)	($0.11^{+0.53}_{-0.10}, 0.89^{+0.10}_{-0.53}, 0$)	200	$199.53^{+4.65}_{-4.54}$	($0.33^{+0.02}_{-0.02}, 0.67^{+0.02}_{-0.02}, 0$)	($0.00^{+0.02}_{-0.00}, 1.00^{+0.00}_{-0.02}, 0$)
				10^3	$1000.00^{+23.29}_{-22.76}$	($0.33^{+0.02}_{-0.02}, 0.67^{+0.02}_{-0.02}, 0$)	($0.00^{+0.06}_{-0.00}, 1.00^{+0.00}_{-0.06}, 0$)

^a Assuming $f_{\tau,S}^{\text{LE}} = f_{\tau,S}^{\text{HE}} = 0$, so $f_{\mu,S}^{\text{LE}} = 1 - f_{e,S}^{\text{LE}}$ and $f_{\mu,S}^{\text{HE}} = 1 - f_{e,S}^{\text{HE}}$.